Contrib Mineral Petrol (2006) 151: 751–768
DOI 10.1007/s00410-006-0091-6

ORIGINAL PAPER

M. J. Flowerdew · I. L. Millar · A. P. M. Vaughan
M. S. A. Horstwood · C. M. Fanning

The source of granitic gneisses and migmatites in the Antarctic Peninsula: a combined U–Pb SHRIMP and laser ablation Hf isotope study of complex zircons

Received: 10 June 2005 / Accepted: 20 March 2006 / Published online: 22 April 2006

Abstract Zircons gneisses and migmatites collected from the Antarctic Peninsula have different core–rim hafnium isotope ratio relationships depending on whether evidence for zircon dissolution is present or absent. Two samples contain inherited zircon that is partially dissolved. In these samples, the $^{176}Hf/^{177}Hf$ rations of the inherited zircon and new magmatic zircon rims are, on average, indistinguishable and consistent with in situ melting. In such cases the hafnium isotopic composition of the melt was probably strongly influenced by the dissolved zircon component at the source. Variation in $^{176}Hf/^{177}Hf$ within the magmatic zircon rims from grain to grain suggests that Hf isotopes were only partially homogenized during melt migration; alternatively, zircon growth may have taken place within small volumes of partial melt. Other samples do not preserve textural evidence for zircon dissolution during melt generation; in these samples the $^{176}Hf/^{177}Hf$ values of the inherited zircon and new magmatic zircon rims are different. The zircon rims apparently suggest a source of less evolved hafnium than that contained within the inherited zircon. Whether this relates to a separate juvenile source or, alternatively, is derived from minerals other than zircon at the source, cannot be resolved. Inherited zircon, irrespective of age, has been strongly influenced by the reworking of a juvenile Late Mesoproterozoic source, suggesting that such crust underlies the Antarctic Peninsula. Our results therefore suggest that Hf isotope analyses provide great potential for future studies investigating the source and processes involved in the generation of crustal melts.

Communicated by I. Parsons

M. J. Flowerdew (✉) · I. L. Millar · A. P. M. Vaughan
British Antarctic Survey, High Cross, Madingley Road, Cambridge CB3 0ET, UK
E-mail: mf@bas.ac.uk
Tel.: +44-115-9363191
Fax: +44-115-9363302

M. S. A. Horstwood · M. J. Flowerdew · I. L. Millar
NERC Isotope Geosciences Laboratories, Kingsley Dunham Centre, Keyworth, Nottingham NG12 5GG, UK

C. M. Fanning
PRISE, Research School of Earth Sciences, The Australian National University, Mills Roads, Canberra, ACT 0201, Australia

Introduction

For most crustal processes zircon grains behave in a refractory way, which makes them unparalleled recorders of the source region history of both magmatic and sedimentary rocks. Inherited zircon grains from crust-derived granitoid and migmatitic rocks are commonly studied in order to characterize their source region (e.g., Clemens 2003). Given their refractory nature, zircon grains can be entrained in, and carried along with, melt during crustal anatexis (Watson and Harrison 1983; Williams and Claesson 1987; Paterson et al. 1992; Clemens 2003). The two most successfully applied techniques in studying the provenance of such inherited zircons involve determining their U–Pb age distribution (Pidgeon and Compston 1992; Williams 1995, 2001; Maas et al. 2001; Tikhomirova 2002; Zeck and Williams 2002; Scherstèn et al. 2004) or their REE chemistry (Hoskin and Schalteggar 2003; Whitehouse and Kamber 2003).

Like the U–Pb system, the Lu–Hf system is refractory in zircon during crustal melting and Hf isotope inheritance has commonly been recognized (e.g., Smith et al. 1987; Corfu and Noble 1992). With the refinement of in situ analysis techniques (Kinny et al. 1991; Thirlwall and Walder 1995) a more rigorous evaluation of the Hf isotope character in complex zircon grains is now possible. In situ measurement of Hf isotopes in zircon has been successfully applied to studies of ancient (Andersen

et al. 2002; Knudsen et al. 2001; Veevers et al. 2005) and modern sedimentary zircon provenance (Griffin et al. 2004), metamorphic gneiss terranes (Halpin et al. 2005) and aspects of igneous petrogenesis (Andersen and Griffin 2004; Griffin et al. 2002). However, the study of the zircon xenocrysts within igneous rocks is largely dedicated to restitic lower crustal material and zircon megacrysts brought to the surface as xenocrysts and xenoliths within kimberlites (Griffin et al. 2000; Zheng et al. 2004). In this study, we describe the growth history, U–Pb age and Hf isotope signature of complex zircons within mid-crustal migmatites and granitic gneisses from four separate localities along the Antarctic Peninsula (Fig. 1). In addition we compare zircon grains from a leucogranite with its proposed source rock. From these analyses we evaluate the benefits of measuring Hf isotopes in xenocrystic zircon in understanding the melted source rocks.

Geology

Traditionally, the Antarctic Peninsula is modeled as having developed as an Andean-style margin from the Mesozoic through the Cenozoic (Suárez 1976; Leat et al. 1995), although more recent work has identified suspect terranes making up the western part of the Peninsula (Vaughan and Storey 2000). Intermittent magmatism, deformation and metamorphism related to subduction beneath the Antarctic Peninsula, affected Mesozoic and pre-Mesozoic basement (e.g., Millar et al. 2002).

Events such as continental breakup (Storey 1991; Storey et al. 1988), extension (Vaughan and Millar 1996; Vaughan et al. 1997) and compression (Vaughan et al. 2002) that possibly involved terrane accretion (Vaughan and Storey 2000) during the development of the Antarctic Peninsula sector of the Gondwana margin, have exposed interior portions of arc basement and continental margin basement in some areas.

Separate episodes of metamorphism and anatexis affected different parts of the Antarctic Peninsula in the Carboniferous, Permian, Middle and Late Triassic (Millar et al. 2002). The Silurian, Late Triassic igneous activity and metamorphism is often viewed as a response to the initiation of subduction along the Antarctic Peninsula (e.g., Leat et al. 1995); however, given the dominantly S-type nature the granitoids, Millar et al. (2002) suggested that this may not be the case. The conditions of metamorphism are poorly understood. However, in northwest Palmer Land (Fig. 1), geothermobarometry from migmatized paragneisses suggests conditions ranging between 800°C at 5–6 kbar and 600°C at 2 kbar (Piercy and Harrison 1991). Piercy and Harrison (1991) proposed that magmatic heating in an arc caused metamorphism, rather than burial and compaction as in a mountain belt. The rocks recording higher pressures and temperatures of metamorphism therefore represent the exposure of deeper crustal levels from within the arc.

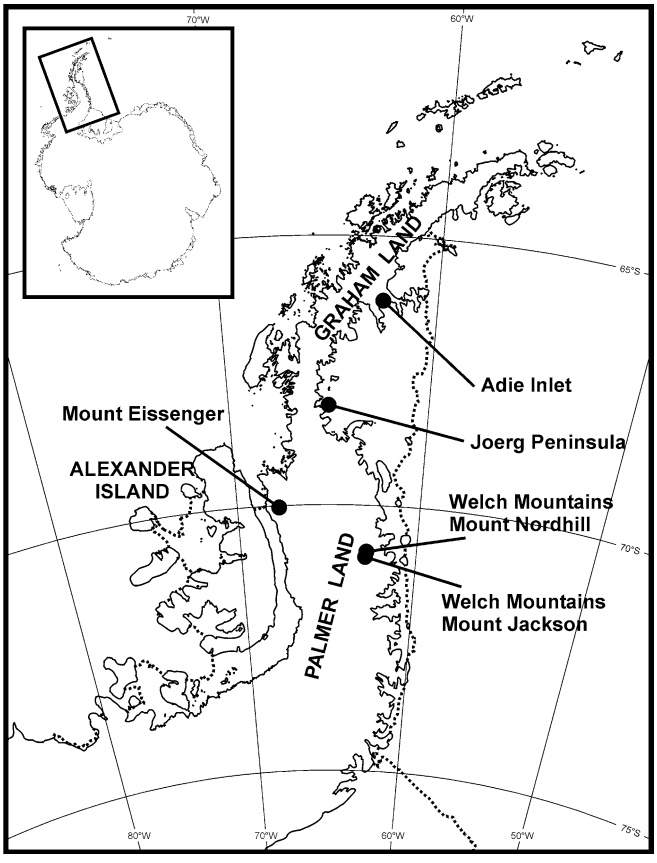

Fig. 1 Sketch map of the Antarctic Peninsula showing sample localities

Analytical methods

U–Pb zircon analyses were performed by sensitive high-resolution ion-microprobe (SHRIMP) at the Australian National University, Canberra. The analytical procedure follows that reported by Williams (1998) and references therein, and is only briefly outlined below.

Zircons were separated, using standard heavy liquid and magnetic techniques, from approximately 1 to 2 kg of rock crushed to < 300 μm. Following handpicking, the zircons were mounted in epoxy along with a few grains of the 1,099 Ma AS3 zircon standard (Schmitz et al. 2003), and polished to expose the centers of the grains, before optical and Cathodoluminescence (CL) imaging. The mount was cleaned and coated with an 80 μm layer of gold and then introduced into the ion-microprobe. Analysis was carried out using a focused primary O_2-beam, and secondary ion intensities were measured with an ion-counting detector. A beam diameter of ~30 μm was used, which resulted in pits 1–2 μm deep. Pb/U ratios were calibrated against the zircon standard using the measured UO/U ratios. The ^{204}Pb signal for each analysis assessed the amount of common Pb. Common Pb was not corrected for and is

assumed to be from surface contamination with a composition of present day values for terrestrial Pb. Concordia ages quoted in the text have been calculated using ISOPLOT version 3.1 (Ludwig 1999) using the decay constants recommended by Steiger and Jäger (1977) and are quoted throughout at the 2σ level.

After SHRIMP analysis, the gold coating was removed using tissue and alcohol and the mounts were cleaned before Hf analysis. Hf analyses were performed using a 266 nm Merchantek Nd:YAG laser attached to a VG Axiom multi-collector inductively coupled mass spectrometer at the NERC Isotope Geosciences Laboratory, UK. Analyses were carried out, where possible, on top of the original ion-microprobe-generated pit, so that Hf analysis could be paired with different stages of zircon growth. Where it was not possible to do so, CL images were used to locate areas of zircon likely to have the same age. The overall analytical approach followed closely that of Horstwood et al. (2003), but with the following modifications for Hf analysis of zircon.

Ablations of 50 μm diameter pits were achieved using a laser beam with a 10 Hz repetition rate and energy of ca. 40 J cm^{-2}. Where possible, 75 ratios of 1 s integrations were collected. However, many analyses were targeted at small inherited cores and thin zircon rims, and suitable material permitted only approximately 20–30 s of data collection. Each analysis typically resulted in a pit depth of approximately 50 μm. A Ta monitor solution was aspirated via a Cetac Technologies Aridus desolvating nebuliser into a modified laser cell (Horstwood et al. 2003), so that the instrument settings and gas flows for both the aspirated and ablated material could be optimized. Additionally, by centering on the stable, aspirated Ta signal, rather than the unstable laser-ablated Hf signal, the centering routine is accurate and the amount of zircon available for Hf data acquisition is maximized.

Masses 172, 173, 175, 176, 177, 178, 179, 180 and 181 were collected in static collection mode in Faraday cups, with mass 177 occupying the axial collector. Data were corrected for mass bias using an exponential law and a value of 0.7325 for $^{179}Hf/^{177}Hf$. Laser induced isotope fractionation during ablation was not evident. Such fractionation was monitored using the $^{178}Hf/^{177}Hf$ and $^{180}Hf/^{177}Hf$ stable isotope ratios, which for the 91,500 zircon standard yielded values of 1.88664 ± 42 (2 SD, $n = 41$) and 1.46710 ± 23 (2 SD, $n = 41$), respectively. JMC 475 standard solution was run during of analyses and yielded 0.282133 ± 24 (2 SD, $n = 27$). Subsequently, our unknown analyses were normalized relative to the accepted value for JMC 475 of 0.28216 (Nowell et al. 1998). This low value is within error of the laboratory 8 month average for the JMC 475 standard solution, which yields a value of 0.282146 ± 74 ppm, and may relate to aspiration via the Cetac Technologies Aridus desolvating nebuliser. A total of 41 analyses of the 91,500 zircon standard (with an accepted $^{176}Hf/^{177}Hf$ of ~0.28230; Wiedenbeck et al. 1995; Woodhead et al. 2004), were acquired intermittently during the analytical session, which after reduction and normalization to the JMC475 standard, gave $^{176}Hf/^{177}Hf = 0.282310 \pm 66$ (± 2 SD, $n = 41$). Data were reduced off-line in a time-resolved fashion so that any changes in $^{176}Hf/^{177}Hf$ that may correspond to ablation though different growth zones (or occasionally through the grain into the epoxy mount) can be identified.

Corrections for the Ta aspirated into the laser cell were performed by way of a simple reverse mass-biased corrected (using $^{179}Hf/^{177}Hf$) subtraction of ^{180}Ta based on the measured ^{181}Ta peak. Ta-doped JMC475 standard gave 0.282130 ± 30 (2 SD, $n = 12$), indistinguishable from the results obtained from undoped JMC475 (see above). ^{180}Ta typically resulted in 3,000 counts s^{-1}, approximately 0.005% of the 180 beam, making the ^{180}Ta interference insignificant.

Correction for the significant ^{176}Yb and ^{176}Lu interferences on the ^{176}Hf peak following the method outlined by Thirlwall and Walder (1995) and Nowell and Parrish (2001), which has been successfully adopted in a variety of Hf laser-ablation studies of zircon (e.g. Griffin et al. 2000; Andersen et al. 2002; Griffin et al. 2002; Zheng et al. 2004; Veevers et al. 2005). Mass bias corrections for Yb were assumed to be similar to that for the measured $^{179}Hf/^{177}Hf$ and although Chu et al. (2002) demonstrated the mass bias behavior of Hf and Yb were subtly different, they concluded that the assumption was appropriate for such mass bias correction. For our analyses, Yb was corrected for $^{176}Yb/^{173}Yb = 0.795238$. Yb-doped JMC475 solutions with Yb/Hf of 0.05 and 0.1 yielded 0.282126 ± 26 (2 SD, $n = 11$) and 0.282132 ± 16 (2 SD, $n = 10$), respectively, within error of the undoped and Ta-doped JMC 475 solutions (see above). The same protocol was followed to establish a Lu correction factor of $^{176}Lu/^{175}Lu$ of 0.026522. Lu correction proved insignificant given the small Lu concentrations of the analyzed zircons. However, εHf and t_{DM} model ages (Table 2) were always calculated on the Lu uncorrected ratios.

Our Yb corrections were deemed appropriate on three counts. Firstly, the Yb-doped JMC475 solution gave $^{176}Hf/^{177}Hf$ indistinguishable to those analyses without doping. Secondly, laser ablation analyses of the 91500 zircon standard gave $^{176}Hf/^{177}Hf$ within error of the currently accepted values for the standard. Thirdly, time-resolved analysis allows variations in Yb concentration to be identified as the sample is ablated. During several analyses three-fold changes in Yb concentration did not result in any change in the Yb-corrected $^{176}Hf/^{177}Hf$ (Fig. 2).

Field relations, petrography and geochronology

Adie Inlet gneiss, R.349.2

The Adie Inlet gneiss (Pankhurst 1983) forms part of a wider area of intermittent exposure of mixed lithology

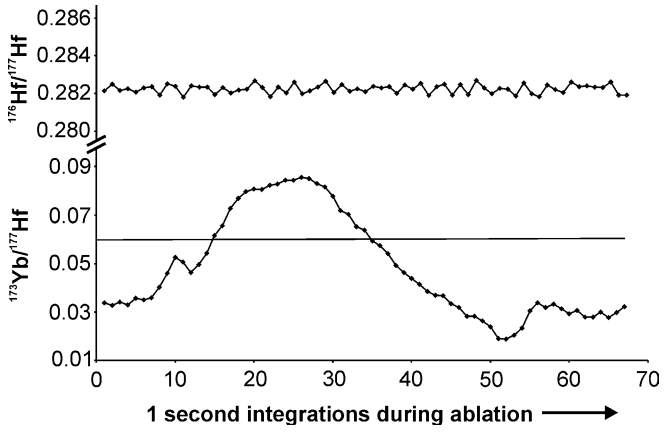

Fig. 2 Change of $^{176}Hf/^{177}Hf$ (*top*) and $^{173}Yb/^{177}Hf$ (*bottom*) during ablation analysis 32.1 from sample R.4293.1 (Table 2). The increase of $^{173}Yb/^{177}Hf$, caused by an increase of Yb concentration but with no corresponding increase in Hf concentration, does not change the $^{176}Hf/^{177}Hf$. Portions of the ablation with $^{173}Yb/^{177}Hf$ values above and below 0.06 are indistinguishable, yielding average $^{176}Hf/^{177}Hf$ values of 0.28226 ± 9 and 0.28228 ± 7, respectively

that stretches from Adie Inlet to Gulliver Nunatak on the Eastern Coast of Graham Land (Fig. 1). Early Jurassic volcanics, with numerous gneissic xenoliths, structurally overlie the gneiss exposures (Thomson and Pankhurst 1983). The analyzed sample is a sub-rounded, coarse-grained enclave, composed of porphyroblastic K-feldspar within a K-feldspar–plagioclase–quartz–biotite–muscovite matrix, hosted in a leucogranite gneiss matrix. It may represent restite within the gneiss. Both gneiss and enclave are migmatized. Zircons are variously elongate and form multifaceted crystals. CL images reveal that most grains comprise a core, surrounded by a thin 20 μm overgrowth (Fig. 3a), such that the size and shape of the core determines the size and shape of the zircon. Overgrowths are dark in CL and sometimes exhibit fine-scale growth zonation. Cores vary from angular and broken to more commonly rounded or sub-rounded and are interpreted to be inherited. The CL of the inherited cores is highly variable but most grains have growth zoning patterns that are terminated by the later relatively non-luminescent overgrowth. A few grains show an irregular margin between core and rim (e.g. grain 21, Fig. 3a) but in the great majority of grains, the boundary between core and rim is regular and sharp.

U–Pb geochronology, previously performed by Millar et al. (2002) using SHRIMP, of the inherited zircon cores gave age clusters at ca. 500–550 Ma and 1,000–1,050 Ma (Fig. 4a). The ages of the inherited zircons are similar in age to detrital zircon populations from nearby sediments (BAS unpublished data), and suggest that the enclave has a sedimentary protolith. The non-luminescent rims gave a Late Permian age of 258 ± 3 Ma (Millar et al. 2002) confirming a Permian age for migmatization, previously determined by Rb–Sr and K–Ar biotite mineral ages (Rex 1976; Pankhurst 1983). However, it must be noted that both this enclave and the host gneiss have anomalously high $^{87}Sr/^{86}Sr$ compared with the majority of the Adie Inlet gneisses. This led Pankhurst (1983) to speculate that the protolith at this locality was at least partly sedimentary, with an ancient provenance. Sm–Nd analyses of this and other similar granitoid gneisses from Adie Inlet broadly support this interpretation and give depleted mantle Nd model ages of ca. 1,550 Ma with εNd of −7 at ca. 258 Ma (Millar et al. 2001; Hole 1986). Hole (1986) concluded, on the basis of the Sr and Nd data, combined with major and trace element geochemistry, that the gneisses represent partial melts from a garnet-rich intermediate metamorphic rock at depth.

Joerg Peninsula gneiss, R.2602.1

Gneisses from the Joerg Peninsula (Fig. 1) are divided into three lithological types: biotite gneiss, granodioritic gneiss and granite gneiss (Hole et al. 1991). The selected sample of granite gneiss is foliated and contains small porphyroblasts of K-feldspar in a leucocratic matrix comprising plagioclase, muscovite, biotite and quartz (Hole 1986). The gneisses are cut by the relatively undeformed Late Triassic 206 ± 6 Ma (Rb–Sr whole rock isochron: Hole et al. 1991) Pylon Point granite, which yields a U–Pb zircon age indistinguishable from the Rb–Sr age (BAS unpublished data).

Zircons are prismatic, euhedral and have high aspect ratios of up to 5:1. Under CL, the zircons exhibit complicated core and rim structures (Fig. 3b). Rounded cores are only rarely present (e.g. grains 3 and 5, Fig. 3b). More common are angular cores with fine-scale, strongly luminescent growth zoning (e.g. grains 8 and 9, Fig. 3b). The contacts between these luminescent cores and the ubiquitous relatively non-luminescent rims are angular, sharp, and cut across the zonation patterns in the cores. Grains 3 and 5 (Fig. 2b) both have rounded cores that are surrounded by a bright, zoned "outer" core and have an angular contact with the dark rim. Rims, although dark, exhibit faint fine-scale growth zoning, and often comprise the majority of the zircon grain. In addition, the sample contains euhedral, prismatic grains up to 200 μm-in length, which have no cores and have similar characteristics to the dark rims (Fig. 3b). Similar grains make up around 15–20% of the total zircon population, suggesting that nucleation of new zircon occurred at the same time that the CL-dark zircon rims grew.

Prior to this study, the best estimate of the age of the Joerg Peninsula gneiss was 236 ± 7 Ma (mid-Triassic; Rb–Sr whole-rock isochron: Hole et al. 1991). Our new SHRIMP analyses from rims do not yield a concordia age due to some common Pb in the analyses. However, a weighted mean of the $^{206}Pb/^{238}U$ ages yields a Mid-Triassic age of 237 ± 2 Ma (Fig. 5a). Five cores yield

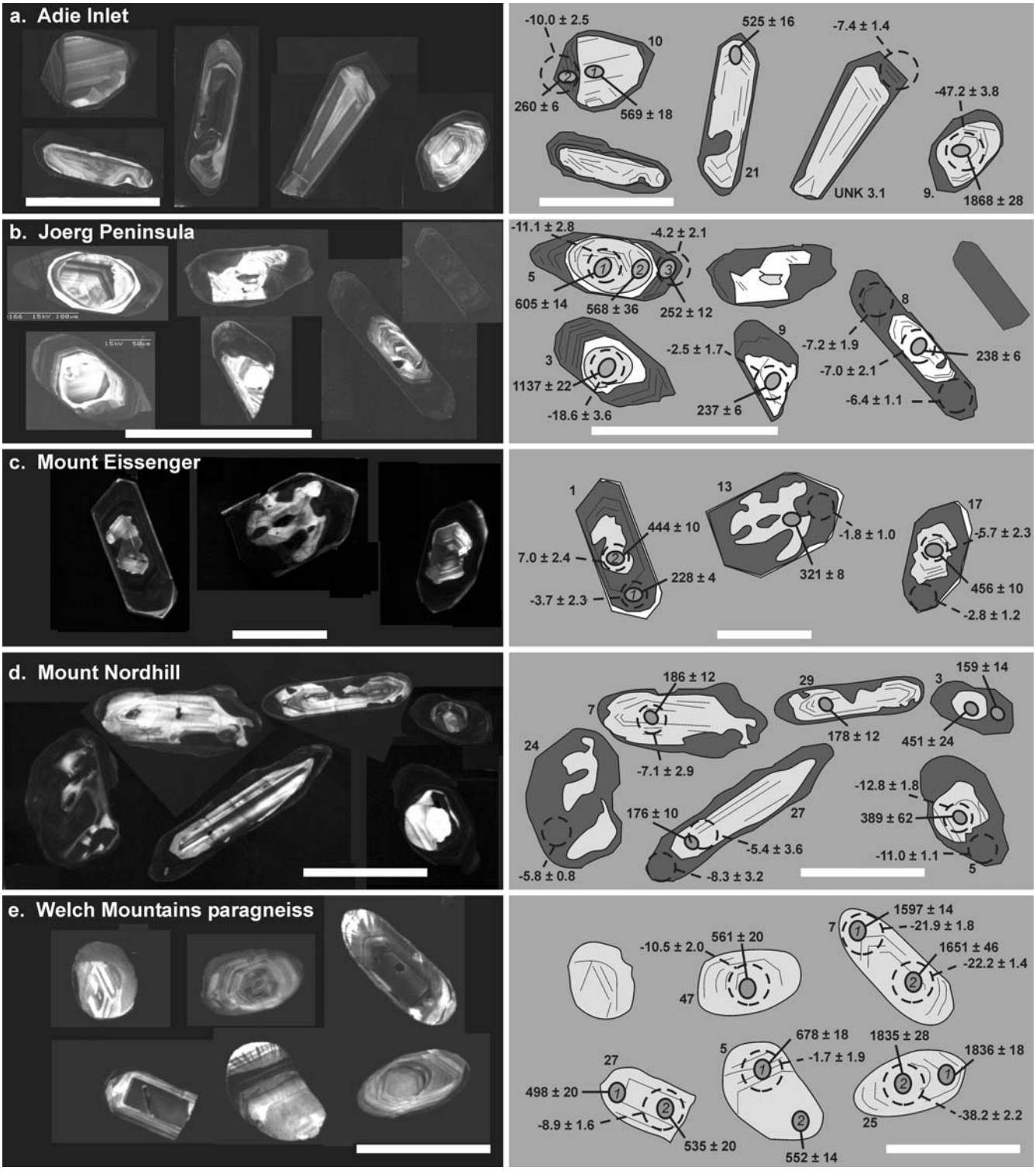

Fig. 3 Cathodoluminescence images (*black panels*, *left*) and their interpretation (*grey panels*, *right*) for zircons from **a** Adie Inlet, **b** Joerg Peninsula, **c** Mount Eissenger, **d** Mount Nordhill and **e** Welch Mountains paragneiss. Interpretations show inherited or detrital cores in *pale grey*, zircon that grew during migmatization in *dark grey*. Areas in white are inner rims for the Joerg Peninsula sample but later rims for the Mount Eissenger sample. Individual U–Pb SHRIMP spots are shown by (*grey ellipses*) and corresponding ages are given ($^{206}Pb/^{238}U$ ages except where the age is > 1500 Ma where the $^{207}Pb/^{206}Pb$ age is given). *Dashed circles* indicate the location of the Hf analyses with the corresponding εHf value at the time of migmatization (Adie Inlet, t = 258 Ma; Joerg Peninsula, t = 238 Ma; Mount Eissenger, t = 227 Ma and for both Mount Nordhill and Welch Mountains, t = 166 Ma). All errors are given at the 2σ level. The number adjacent to individual grains identifies the grain as indicated in Tables 1 and 2. Scale bar is 200 μm

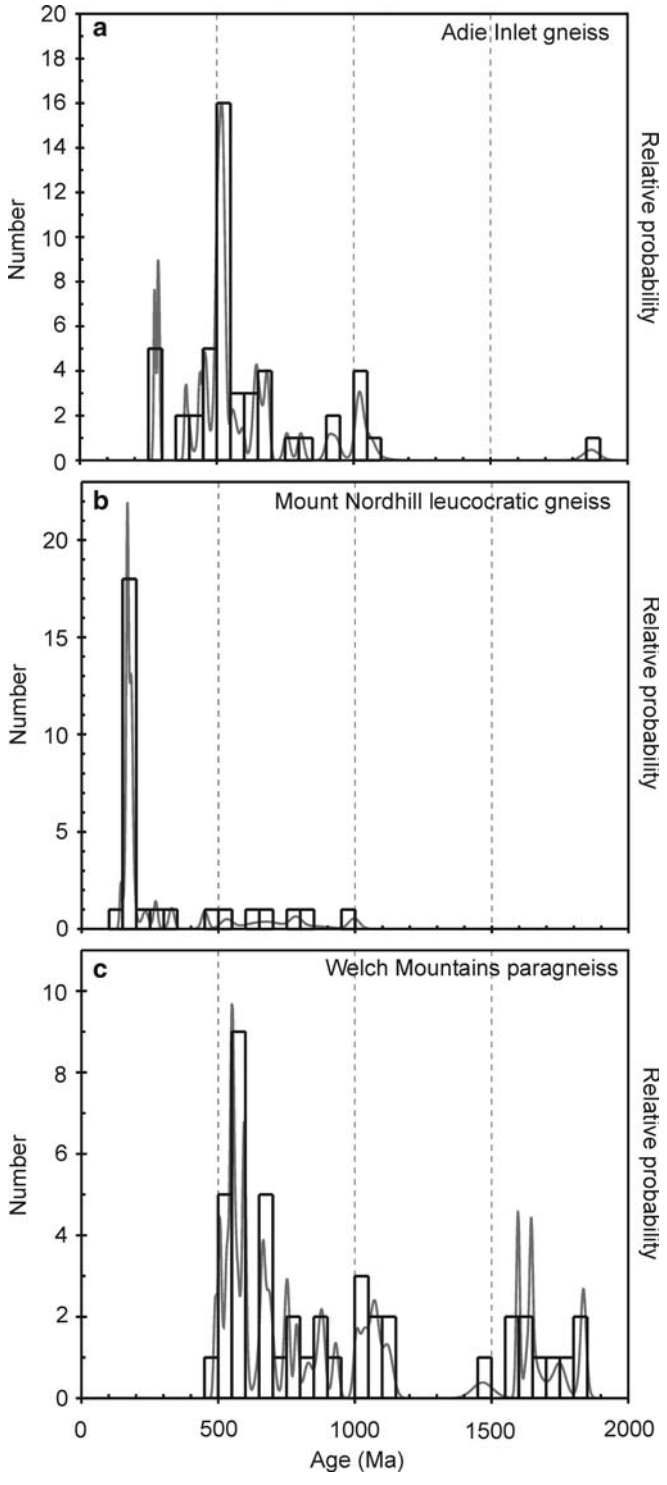

Fig. 4 Relative probability plots for inherited zircon U–Pb ages for **a** Adie Inlet gneiss (data from Millar et al. 2002), **b** inherited zircon from the Mount Nordhill leucogranite sheet and **c** detrital zircons from the Welch Mountains paragneiss. Zircons analyses with a high discordance (>10%) are not included. For ages less than 1,500 Ma the $^{206}Pb/^{238}U$ age is used for grains older than 1,500 Ma the $^{207}Pb/^{206}Pb$ age is used

$^{206}Pb/^{238}U$ ages of 497 ± 12 Ma, 568 ± 36 Ma, 605 ± 14 Ma, 1037 ± 22 Ma and a $^{207}Pb/^{206}Pb$ age of 1,687 ± 14 Ma (Table 1).

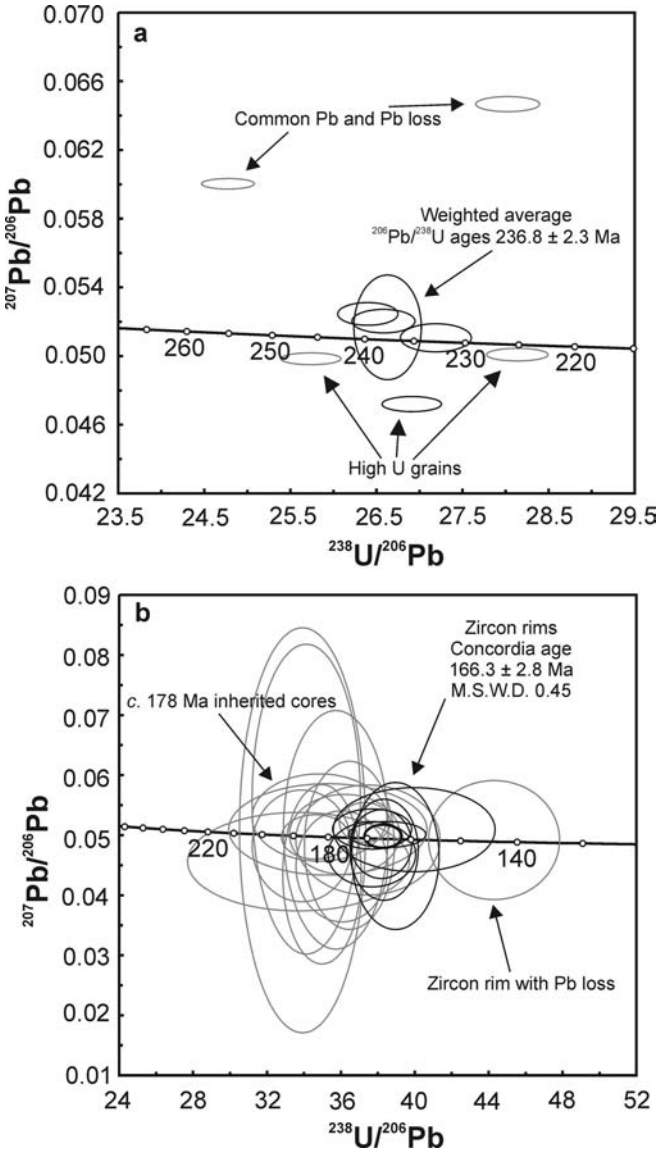

Fig. 5 U–Pb concordia diagrams showing the young zircon analyses from **a** the Joerg Peninsula granite gneiss and **b** Mount Nordhill gneisses leucocratic sheet. *Black ellipses* are used in the age calculations and are interpreted to date migmatization or magmatism. *Grey ellipses* are discounted from age calculations either as they contain large proportions of common Pb, have suffered Pb loss, are discordant, or are interpreted to be inherited cores

Mount Eissenger leucosome, R.5257.1

Layered, polyphase folded gneisses crop out at the eastern end of Mount Eissenger (Fig. 1) and on the southeast flank of Mount Allan, and are separated from Cretaceous gabbro by a high-strain zone (Vaughan and Millar 1996). The gneisses have a banded appearance with centimeter-scale compositional layering, and locally contain angular mafic fragments as well as more rounded inclusions of rhyolitic and pelitic material. These inclusions probably represent xenoliths of wall rock incorporated in individual magmatic sheets before they recrystallized to gneiss (APM Vaughan unpublished

data). In other areas, field relations suggest that the leucocratic bands within the gneiss are leucosomes that possibly represent in situ melting of an orthogneiss protolith (APM Vaughan unpublished data). Zircons were separated from one such leucocratic band, which is granitic in composition, medium-grained, and has undergone pervasive post-crystallization ductile deformation.

The zircons are large (commonly > 300 μm in length), euhedral, stubby to prismatic, and show complicated internal structures under CL (Fig. 3c). The centers of grains contain moderately bright cores with fine-scale growth zonation overgrown by relatively non-luminescent zircon with diffuse growth zonation. The contact between the core and the surrounding zircon is convoluted and highly lobate (e.g. grain 13, Fig. 3c). Non-luminescent zircon also forms acicular grains without any inherited core. The non-luminescent overgrowths are in turn ubiquitously overgrown by thin, < 10 μm rims with moderate luminescence and growth zoning (e.g. grain 1, Fig. 3c). These outer rims form the well-developed crystal facets. The contacts of these rims cut across growth zones within the inner rims, suggesting that the latter were partially dissolved and resorbed before the outer rims grew.

SHRIMP analyses documented in Millar et al. (2002) show that the inherited cores have a simple age distribution, confirming that the gneiss has an igneous protolith with an age of 422 ± 18 Ma (Late Silurian). Formation of the non-luminescent overgrowths occurred at 228 ± 3 Ma (mid–Late Triassic) and was followed by a final stage of zircon growth accompanying metamorphism in Late Triassic–Early Jurassic times at ca. 202 Ma (Millar et al. 2002). Sm–Nd analysis of this rock yields a depleted mantle Nd model age of ca. 1,030 Ma with εNd of −0.1 at the time of migmatization, ca. 228 Ma (Millar et al. 2001).

Mount Nordhill, leucocratic gneiss, R.4552.9

A complex of paragneiss disrupted by gneissic leucogranite sheets, gneissic K-feldspar megacrystic granites and homogeneous biotite-orthogneisses, is exposed at Mount Nordhill (Fig. 1; Wever et al. 1995). The selected sample is from a gneissic leucocratic sheet containing the assemblage K-feldspar, quartz, plagioclase and biotite (Wever et al. 1994). Zircons from are subhedral and range in shape from stubby to prismatic, and in size from ca. 50 μm to > 300 μm. Under CL, all grains exhibit cores and rims; for approximately 70% of the grains, the cores make up a large proportion of the grain and subsequently control its size and shape (Fig. 3d). In most grains the luminescent cores exhibit a growth-zoning pattern and their contacts with the generally featureless non-luminescent rims is highly irregular (e.g. grain 24, Fig. 3d). This texture strongly resembles that of the Mount Eissenger sample (above). New SHRIMP U–Pb analyses of zircon rims yielded a mid-Jurassic concordia age of 166 ± 3 Ma (Fig. 5b). These are interpreted to have grown from a melt. The highly resorbed cores include an inherited component that is dominated by latest Early Jurassic ages, and yield a concordia age of 178 ± 3 Ma. Other ages for the inherited cores range from ca. 215 Ma up to ca. 1,500 Ma (Fig. 4b; Table 1). Depleted mantle Nd model ages of ca. 1,605 Ma and εNd values of −8.4 at the age of emplacement at ca. 166 Ma, together with the peraluminous chemistry for the rock, suggest that the melt may be derived through crustal anatexis of the paragneisses that they cut, or similar rock nearby (e.g. sample R.4293.1 detailed below: Wever et al. 1994; Millar et al. 2001).

Welch Mountains paragneiss, R.4293.1

Quartzitic paragneiss forming part of a sequence of quartz-rich to semi-pelitic migmatitic paragneiss, crops out at Solem Ridge near Mount Jackson in the Welch Mountains (Fig. 1; Singleton 1980). A sheeted complex of gneissic leucogranitic, biotite orthogneiss and granite pegmatite intrudes the paragneisses. These paragneisses and similar rocks in the vicinity are thought to be the source for the gneissic leucogranite sheets exposed at Mount Jackson and Mount Nordhill (R.4552.9 above). The paragneiss (R.4293.1) yields a 1,707 Ma depleted mantle model age and εNd of −9.6 at 166 Ma (Millar et al. 2001). Analyses of paragneiss throughout the Mount Nordhill and Mount Jackson area all have a similar isotopic character (Millar et al. 2001).

Zircons from the paragneiss are rounded and commonly have a pitted surface. Under CL the grains show a wide variety of brightness and zoning characteristics (Fig. 3e). The rounded nature of the grains, coupled with the dissimilar and varied CL zoning characteristics from grain to grain, suggest that these grains were worn and abraded during sediment transport and suggest a lithologically varied source for the sedimentary protolith. No new zircon grew during metamorphism, and zircon dissolution during metamorphism is thought unlikely as pitting of the zircon surface is thought to be a product of sedimentary abrasion. New SHRIMP U–Pb ages show a detrital zircon age distribution that is dominated by ca. 500 Ma to ca. 650 Ma zircons, but also has important contributions of zircons with age ranges between ca. 1,000–1,150 Ma and ca. 1,600–1,800 Ma (Fig. 4c).

Hf isotope data

Adie Inlet gneiss

Circa 258 Ma rims from three separate zircon grains and two other zircon grains where the time-resolved

Table 1 U–Pb SHRIMP zircon geochronology

Spot[a]	Analysis[b]	U (ppm)	Th (ppm)	Pb (ppm)	Th/U	$f^{206}Pb$[c] (%)	$^{238}U/^{206}Pb$	±	$^{207}Pb/^{206}Pb$	±	$^{206}Pb/^{238}U$ age (Ma)	± Ma[d]	$^{207}Pb/^{206}Pb$[e] age (Ma)	± Ma[d]
R.2602.1 Joerg Peninsula														
14.1[f]	*r*	*1,887*	*468*	*49*	*0.25*	*1.71*	*28.0250*	*0.3028*	*0.0647*	*0.0004*	*222*	*2*	*764*	*12*
1.1	r	2,486	23	61	0.01	< 0.01	28.1360	0.2920	0.0501	0.0003	225	2	199	14
11.1[g]	r	1,598	933	47	0.58	0.01	27.1900	0.3369	0.0511	0.0007	233	3	244	30
4.1[f,g]	r	2,115	3,232	75	1.53	< 0.01	26.9110	0.2819	0.0472	0.0004	236	2	59	18
9.1[g]	r	429	256	13	0.60	0.09	26.6300	0.3200	0.0517	0.0025	237	3	271	110
8.1[g]	r	707	487	22	0.69	0.13	26.5820	0.2988	0.0520	0.0006	238	3	287	25
6.1[g]	r	876	963	30	1.10	0.18	26.4000	0.2858	0.0525	0.0005	239	3	305	23
2.1[f]	r	5,007	485	136	0.10	< 0.01	25.7380	0.2855	0.0498	0.0003	246	3	188	13
5.3[f]	*r*	*5,328*	*190*	*146*	*0.04*	*1.13*	*24.7750*	*0.2512*	*0.0600*	*0.0003*	*252*	*3*	*605*	*9*
13.1[f]	c	560	125	33	0.22	< 0.01	12.5150	0.1514	0.0550	0.0006	497	6	411	23
5.2	c	483	101	33	0.21	< 0.01	10.9370	0.3492	0.0532	0.0044	568	18	336	186
5.1[f]	c	776	551	63	0.71	0.27	10.1400	0.1140	0.0621	0.0006	605	7	678	19
3.1	c	639	482	93	0.76	< 0.01	5.7615	0.0626	0.0701	0.0036	1,037	11	930	105
10.1	c	260	74	65	0.29	< 0.01	3.0345	0.1420	0.1035	0.0004	1,838	75	1,687	7
R.4552.9 Mount Nordhill														
13.1	r	2,492	252	51	0.10	2.13	44.290	1.449	0.0492	0.0041	144	5	157	193
3.1[g]	r	1,845	268	42	0.15	1.18	39.967	1.788	0.0509	0.0029	159	7	237	130
20.1[g]	r	6,693	209	155	0.03	3.50	38.953	0.965	0.0465	0.0050	163	4	26	258
1.1[g]	r	2,217	11	52	0.00	0.01	38.501	0.856	0.0501	0.0009	165	4	200	41
19.1[g]	r	1,225	1,927	43	1.57	0.52	38.337	0.756	0.0476	0.0034	166	3	78	172
2.1[g]	r	2,064	18	49	0.01	0.38	38.185	0.673	0.0485	0.0023	167	3	124	114
18.1[g]	r	3,130	148	76	0.05	0.07	37.690	0.875	0.0510	0.0014	169	4	242	62
22.1[g]	r	1,128	1,205	36	1.07	0.28	37.679	0.969	0.0468	0.0022	169	4	41	113
9.1	c	2,192	119	53	0.05	1.38	37.466	1.595	0.0492	0.0037	170	7	157	178
12.1	c	1,814	163	45	0.09	0.19	37.294	0.564	0.0521	0.0014	171	3	291	59
4.1	*c*	*1,575*	*839*	*45*	*0.53*	*40.31*	*36.828*	*2.165*	*0.0532*	*0.0390*	*173*	*10*	*338*	*1,660*
33.1	c	842	959	23	1.14	1.12	36.457	0.994	0.0483	0.0057	174	5	114	279
16.1	c	1,346	244	35	0.18	0.74	36.203	1.220	0.0501	0.0027	176	6	200	127
27.1	c	466	393	14	0.84	0.65	36.056	1.015	0.0448	0.0038	176	5	−66	206
29.1	c	627	583	17	0.93	1.76	35.727	1.158	0.0509	0.0081	178	6	236	368
34.1	c	725	307	21	0.42	0.09	35.295	2.191	0.0510	0.0031	180	11	239	141
1.2	c	401	170	11	0.42	0.86	34.976	0.866	0.0435	0.0061	182	4	−139	347
16.1	c	864	702	28	0.81	0.06	34.844	1.491	0.0529	0.0030	182	8	326	127
11.1	c	628	612	21	0.97	0.10	34.628	0.754	0.0497	0.0015	184	4	181	71
7.1	*c*	*369*	*212*	*12*	*0.57*	*1.15*	*34.125*	*1.197*	*0.0560*	*0.0105*	*186*	*6*	*452*	*418*
26.1	*c*	*260*	*220*	*8*	*0.85*	*0.87*	*33.922*	*1.394*	*0.0508*	*0.0138*	*187*	*8*	*233*	*626*
17.1	c	157	171	6	1.09	0.22	33.886	1.096	0.0482	0.0038	187	6	110	186
21.1	c	1,041	450	31	0.43	0.32	33.708	2.453	0.0456	0.0034	188	14	−24	178
8.1	*c*	*433*	*181*	*13*	*0.42*	*16.64*	*33.394*	*1.083*	*0.0453*	*0.0226*	*190*	*6*	*−41*	*1,212*
21.1	*c*	*828*	*743*	*30*	*0.90*	*6.34*	*29.463*	*0.889*	*0.0454*	*0.0163*	*215*	*6*	*−32*	*872*
15.1[f]	c	2,060	49	70	0.02	1.06	27.148	1.380	0.0627	0.0021	233	12	697	73
31.1[f]	c	478	204	22	0.43	0.22	23.285	0.648	0.0696	0.0040	271	7	915	123
6.1	c	345	127	18	0.37	0.08	19.086	0.574	0.0582	0.0034	329	10	537	133
5.1	*c*	*90*	*57*	*6*	*0.63*	*14.91*	*16.0737*	*1.3026*	*0.0770*	*0.0486*	*389*	*31*	*1,120*	*2,454*
3.2	c	754	304	55	0.40	0.06	13.815	0.366	0.0553	0.0014	451	12	423	58
22.1	*c*	*679*	*284*	*59*	*0.42*	*0.63*	*11.766*	*1.392*	*0.0659*	*0.0034*	*526*	*60*	*803*	*113*
15.2	c	946	126	81	0.13	0.12	11.652	0.503	0.0780	0.0014	531	22	1,146	37
19.1	c	587	115	58	0.20	0.25	9.800	0.747	0.0607	0.0039	626	46	629	144
18.1	c	378	94	42	0.25	0.84	8.797	0.553	0.0718	0.0055	694	42	980	163
15.1[f]	c	694	236	91	0.34	0.16	7.735	0.220	0.0766	0.0012	784	21	1,109	32
28.1	c	296	60	40	0.20	0.20	7.275	0.646	0.0739	0.0055	830	70	1,038	157
23.1[f]	c	483	91	79	0.19	0.02	5.978	0.128	0.0790	0.0011	997	20	1,173	27
10.1[f]	*c*	*351*	*28*	*95*	*0.08*	*0.02*	*3.873*	*0.121*	*0.1950*	*0.0032*	*1,481*	*42*	*2,785*	*27*
R.4293.1 Welch Mountains														
30.1[f]		*2,630*	*140*	*193*	*0.05*	*1.00*	*15.334*	*0.330*	*0.0630*	*0.0006*	*407*	*8*	*708*	*21*
37.1[f]		1,479	5	133	0.00	0.27	12.646	0.158	0.0594	0.0004	491	6	582	15
27.1[f]		*152*	*72*	*16*	*0.48*	*0.76*	*12.444*	*0.262*	*0.0634*	*0.0017*	*498*	*10*	*721*	*57*
17.1		993	83	57	0.08	< 0.01	12.259	0.129	0.0556	0.0024	506	5	437	98
2.1[f]		128	122	9	0.95	0.52	12.154	0.195	0.0617	0.0008	510	8	665	28
45.1		957	252	102	0.26	0.03	11.626	0.151	0.0583	0.0007	532	7	540	27
27.2[f]		448	340	54	0.76	0.27	11.562	0.232	0.0602	0.0007	535	10	611	26
24.1[f]		140	61	10	0.44	0.59	11.235	0.150	0.0639	0.0012	550	7	737	40
11.1		505	894	46	1.77	0.02	11.217	0.144	0.0589	0.0007	551	7	565	26
5.2		736	9	45	0.01	0.09	11.191	0.147	0.0596	0.0003	552	7	588	12

Table 1 (Contd.)

Spot[a]	Analysis[b]	U (ppm)	Th (ppm)	Pb (ppm)	Th/U	$f^{206}Pb^c$ (%)	$^{238}U/^{206}Pb$	±	$^{207}Pb/^{206}Pb$	±	$^{206}Pb/^{238}U$ age (Ma)	± Ma[d]	$^{207}Pb/^{206}Pb$[e] age (Ma)	± Ma[d]
13.1[f]		206	75	14	0.36	0.31	11.171	0.142	0.0614	0.0007	553	7	652	24
47.1		464	148	53	0.32	0.09	11.006	0.201	0.0601	0.0012	561	10	608	43
35.1[f]		636	97	70	0.15	0.57	10.775	0.173	0.0640	0.0008	572	9	743	28
34.1[f]		67	28	8	0.42	0.61	10.658	0.314	0.0643	0.0017	578	16	752	58
4.1		2,547	102	171	0.04	0.42	10.339	0.108	0.0631	0.0017	595	6	711	58
18.1[f]		948	259	68	0.27	< 0.01	10.338	0.112	0.0587	0.0003	595	6	555	10
39.1[f]		*615*	*148*	*72*	*0.24*	*1.04*	*10.267*	*0.152*	*0.0684*	*0.0026*	*599*	*8*	*881*	*80*
43.1[f]		827	114	101	0.14	< 0.01	9.845	0.124	0.0585	0.0005	624	7	547	20
46.1[f]		*205*	*49*	*26*	*0.24*	*1.50*	*9.331*	*0.183*	*0.0742*	*0.0017*	*656*	*12*	*1,046*	*46*
42.1		188	49	25	0.26	0.24	9.327	0.279	0.0639	0.0014	657	19	737	45
32.1		912	27	113	0.03	0.35	9.231	0.185	0.0648	0.0012	663	13	767	39
12.1		303	177	27	0.58	0.13	9.212	0.107	0.0630	0.0037	664	7	707	131
5.1[f]		*148*	*42*	*12*	*0.29*	*0.90*	*9.012*	*0.121*	*0.0692*	*0.0008*	*678*	*9*	*906*	*25*
29.1[f]		422	275	65	0.65	< 0.01	8.921	0.130	0.0612	0.0010	685	9	647	37
10.1[f]		*35*	*33*	*3*	*0.95*	*1.92*	*8.792*	*0.162*	*0.0777*	*0.0020*	*694*	*12*	*1,138*	*51*
49.1		284	146	43	0.51	< 0.01	8.742	0.149	0.0622	0.0008	698	11	679	29
22.1		224	108	22	0.48	< 0.01	8.137	0.112	0.0626	0.0009	747	10	694	32
15.1[f]		737	421	74	0.57	< 0.01	8.048	0.092	0.0597	0.0004	755	8	593	16
26.1		721	325	72	0.45	< 0.01	7.699	0.082	0.0605	0.0047	787	8	623	175
31.1[f]		84	31	15	0.36	0.58	7.273	0.153	0.0712	0.0013	830	16	963	39
28.1[f]		*79*	*60*	*16*	*0.76*	*< 0.01*	*7.136*	*0.312*	*0.0585*	*0.0021*	*845*	*35*	*549*	*82*
48.1[f]		819	261	150	0.32	< 0.01	6.963	0.089	0.0656	0.0007	865	10	794	23
1.1[f]		198	82	22	0.42	0.04	6.914	0.104	0.0713	0.0009	871	12	965	26
23.1[f]		474	133	52	0.28	0.02	6.812	0.087	0.0721	0.0007	883	11	988	20
9.1[f]		216	180	31	0.83	0.02	6.442	0.078	0.0794	0.0006	930	10	1,181	15
6.1		594	268	78	0.45	0.02	5.923	0.066	0.0714	0.0004	1,006	10	969	11
20.1[f]		76	52	11	0.69	0.53	5.778	0.085	0.0796	0.0008	1,029	14	1,186	21
40.1		611	324	144	0.53	0.01	5.680	0.090	0.0750	0.0006	1,045	15	1,068	17
3.1		369	197	53	0.53	0.08	5.560	0.066	0.0759	0.0007	1,066	12	1,092	20
14.1		659	186	90	0.28	0.02	5.482	0.066	0.0716	0.0020	1,080	12	975	57
33.1[f]		*32*	*18*	*7*	*0.56*	*2.38*	*5.444*	*0.166*	*0.0854*	*0.0021*	*1,087*	*31*	*1,325*	*48*
38.1[f]		460	152	109	0.33	0.14	5.333	0.113	0.0718	0.0010	1,108	22	980	29
50.1[f]		270	168	70	0.62	0.35	5.250	0.094	0.0809	0.0011	1,124	19	1,218	26
16.1[f]		*1,736*	*569*	*275*	*0.33*	*< 0.01*	*4.916*	*0.051*	*0.0967*	*0.0024*	*1,194*	*11*	*1,561*	*46*
51.1[f]		*230*	*64*	*66*	*0.28*	*0.07*	*4.307*	*0.072*	*0.0734*	*0.0035*	*1,346*	*20*	*1,026*	*100*
41.1		152	113	55	0.74	0.26	3.911	0.110	0.0925	0.0015	1,468	37	1,478	30
21.1[f]		1,007	178	208	0.18	0.01	3.632	0.044	0.1043	0.0025	1,568	17	1,702	45
19.2		830	872	358	1.05	0.04	3.581	0.045	0.1009	0.0007	1,588	18	1,640	13
8.1		1,263	123	257	0.10	0.01	3.577	0.039	0.0986	0.0003	1,589	15	1,598	6
7.2		341	103	124	0.30	0.12	3.518	0.048	0.1015	0.0012	1,613	20	1,651	23
7.1[f]		442	132	100	0.30	0.03	3.400	0.039	0.0986	0.0004	1,662	17	1,597	7
19.1		713	434	173	0.61	0.02	3.398	0.037	0.1012	0.0003	1,663	16	1,646	5
44.1		177	94	74	0.53	0.18	3.272	0.071	0.1071	0.0012	1,719	33	1,751	21
25.2		217	29	87	0.14	< 0.01	3.091	0.046	0.1122	0.0009	1,807	23	1,835	14
25.1		410	237	111	0.58	0.04	3.056	0.034	0.1123	0.0005	1,825	18	1,836	9

All uncertainties are given at the 1σ level and include propagated errors of the standard measurements. Analyses in italics are highly discordant (> 10% outside of the 2σ uncertainty) or have unreasonably large uncertainties

[a]Spot identification number

[b]Portion of zircon analyzed where *r* rim and *c* core

[c]Proportion of ^{206}Pb that is non-radiogenic

[d]Age errors have included the propogated errors of the standard measurement

[e]Preferred when analysis is discordant or has an age > 1,500 Ma

[f]Discordant analysis (if analysis not italicized discordancy is < 10%)

[g]Analysis used in age calculation

portion of the analysis is interpreted to record ablation of the rim, yielded similar $^{176}Hf/^{177}Hf$ ratios (Table 2; Fig. 6a). Only one rim analysis (UNK.1) is out of analytical uncertainty from the other four analyses. The corresponding core analysis from this grain is highly evolved, and inadvertent mixtures between the core and rim during an unpredictable ablation could account for its slightly lower $^{176}Hf/^{177}Hf$ ratio of the rim compared with the other rim analyses. Excluding this analysis, the rims yield $^{176}Hf/^{177}Hf$ of 0.282480 ± 109 (2 SD, n = 4) which corresponds to $\varepsilon Hf_{(258)}$ of −5.0 ± 4.0 (Fig. 6a). Core analyses are variable both in age and $^{176}Hf/^{177}Hf$ (Table 2). Some cores have a $^{176}Hf/^{177}Hf$ value that is indistinguishable from that of the average $^{176}Hf/^{177}Hf$ for the rims (e.g. grains 20 and UNK2; Table 2). Some grains, however, show significant differences between the core and corresponding rim (Fig. 6a). For grain UNK 1, the core

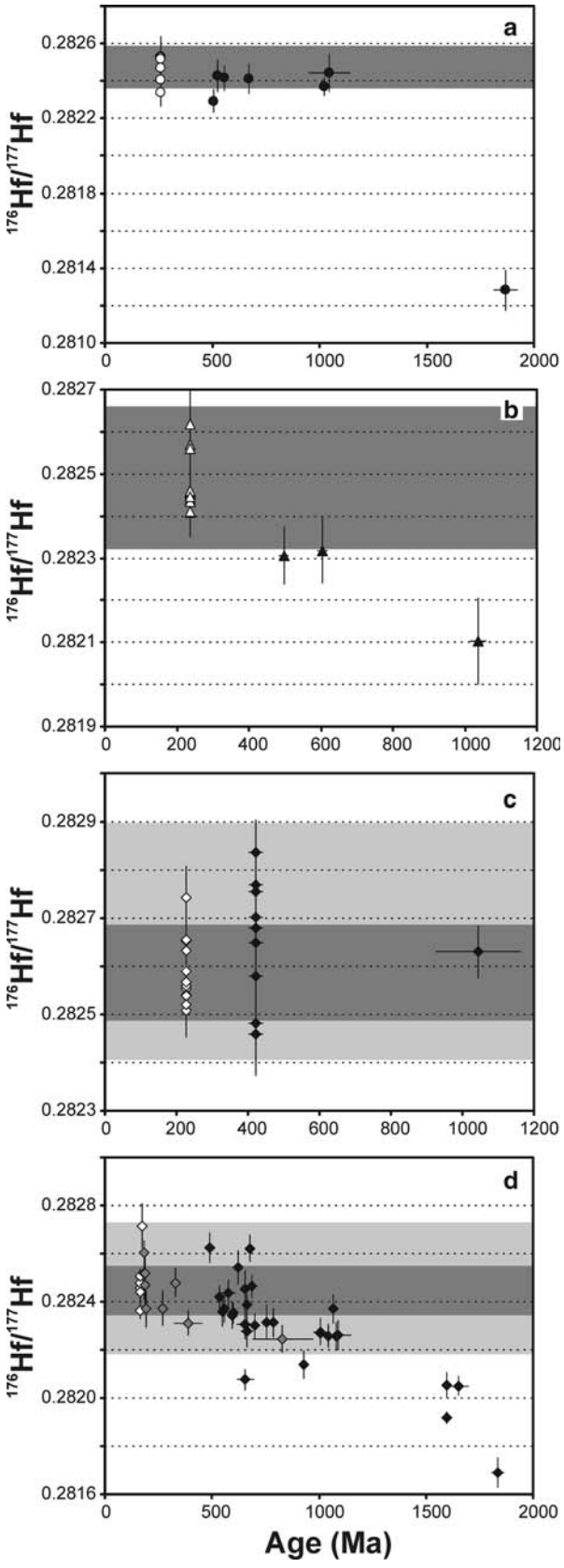

Fig. 6 $^{176}Hf/^{177}Hf_{(t)}$ versus $^{206}Pb/^{238}U$ age plots of zircons from the studied granites and migmatites. **a** *Solid circles*: Adie Inlet inherited. *Open circles*: Adie Inlet rims. **b** *Solid triangles*: Joerg inherited. *Open triangles*: Joerg rims. **c** *Solid diamonds*: Mount Eissenger inherited. *Open diamonds*: Mount Eissenger rims. **d** *Solid diamonds*: Welch Mountains detrital. *Grey diamonds*: Mount Nordhill inherited. *Open diamonds*: Mount Nordhill rims. *Deep grey bands* show the two standard deviation limits about the average of the rims from each sample, respectively. *Pale grey bands*, where shown, show the two standard deviation limits about the average of the inherited grains

gave $^{176}Hf/^{177}Hf$ value of 0.281619 ± 81 (2σ) whilst the rim gave $^{176}Hf/^{177}Hf$ of 0.282337 ± 71 (2σ). This corresponds to a difference of 25 epsilon units between the core and the rim analysis, when calculated at 258 Ma.

Joerg Peninsula gneiss

Eight of eleven rims have indistinguishable $^{176}Hf/^{177}Hf$, within analytical uncertainty. The other three rims have higher $^{176}Hf/^{177}Hf$ (Table 2; Fig. 6b). The rims yield a $^{176}Hf/^{177}Hf$ average of 0.282478 ± 142 (2 SD, n = 11) and no distinction can be made between the $^{176}Hf/^{177}Hf$ of the luminescent inner and the non-luminescent outer rims. The $^{176}Hf/^{177}Hf$ variation of the rims equates to an $\varepsilon Hf_{(238)}$ range from −0.4 to −8.0; greater than would be expected through analytical uncertainty alone. The analyzed cores yield lower $^{176}Hf/^{177}Hf$ values than the majority of the zircon rims, the difference being greater than analytical uncertainty (Fig. 6b). For grain 3 the $^{176}Hf/^{177}Hf$ difference between core and rim corresponds to a shift of 11 εHf units at 238 Ma, the crystallization age of the zircon rim.

Mount Eissenger leucosome

The ca. 227 Ma-old, earliest Late Triassic, non-luminescent zircon that overgrows the partially resorbed cores yields an average $^{176}Hf/^{177}Hf$ value of 0.282589 ± 133 (2 SD, n = 13). Many of the rim analyses have $^{176}Hf/^{177}Hf$ values that differ from each other by more analytical uncertainty. Excluding one highly anomalous result (grain 1.1; Table 2) the average is 0.282589 ± 100 (2 SD, n = 12). The highly resorbed ca. 422 Ma Silurian cores yield more variable $^{176}Hf/^{177}Hf$ than the rims but the average $^{176}Hf/^{177}Hf$ value of 0.282654 ± 244 (2 SD, n = 10) is indistinguishable from that of the rims (Fig. 6c). Two of the ten grains where both core and rim were analyzed (grains 12 and Hf grain 2; Table 2) have $^{176}Hf/^{177}Hf$ values which differ by more than analytical uncertainty.

Mount Nordhill leucocratic gneiss and Welch Mountains paragneiss

The $^{176}Hf/^{177}Hf$ ratios for the ca. 166 Ma rims are somewhat variable from grain to grain, with some grains differing by more than analytical uncertainty, but yield an

Table 2 Hf isotope analyses

spot[a]	Analysis[b]	Age[c]	$^{176}Lu/^{177}Hf$	$^{176}Yb/^{177}Hf$	$^{178}Hf/^{177}Hf \pm 2\sigma$		$^{176}Hf/^{177}Hf_m \pm 2\sigma$		$^{176}Hf/^{177}Hf_I$[d]	$\varepsilon Hf_{(t)}$[e]	$\varepsilon Hf_{(mig)}$[e]	$\pm 2\sigma$[e]	t_{DM} (Ma)[f]
R.349.2 Adie inlet													
8.1	r	258	0.00082	0.02685	1.46724	0.00019	0.282529	0.000109	0.282525	−3.1	−3.1	3.9	1,019
UNK 3.1	r[g]	258	0.00154	0.05454	1.46689	0.00018	0.282515	0.000092	0.282508	−3.7	−3.7	3.3	1,059
UNK.1	r[g]	258	0.00157	0.05564	1.46773	0.00057	0.282337	0.000071	0.282330	−10.0	−10.0	2.5	1,312
UNK.6	r[g]	258	0.00468	0.17376	1.46715	0.00011	0.282468	0.000037	0.282446	−5.9	−5.9	1.3	1,229
UNK3.2	r[g]	258	0.00140	0.05242	1.46718	0.00012	0.282409	0.000038	0.282402	−7.4	−7.4	1.4	1,206
3.1	c	507	0.00159	0.06395	1.46702	0.00019	0.282293	0.000060	0.282278	−6.3	−11.6	2.1	1,376
21.1	c	525	0.00096	0.04508	1.46724	0.00019	0.282428	0.000082	0.282419	−0.9	−6.7	2.9	1,164
UNK.2	c[h]	525	0.00082	0.03119	1.46727	0.00016	0.282394	0.000074	0.282386	−2.1	−7.8	2.6	1,207
UNK.4	c[h]	525	0.00195	0.07532	1.46722	0.00020	0.282373	0.000054	0.282354	−3.2	−8.8	1.9	1,275
UNK.8	c[h]	525	0.00136	0.05432	1.46716	0.00014	0.282392	0.000105	0.282379	−2.3	−8.0	3.7	1,227
2.1	c	555	0.00185	0.07407	1.46726	0.00015	0.282415	0.000065	0.282396	−1.1	−7.3	2.3	1,211
19.1	c	673	0.00162	0.06600	1.46728	0.00016	0.282412	0.000079	0.282392	1.4	−7.3	2.8	1,207
22.1	c	1,025	0.00123	0.05049	1.46726	0.00011	0.282370	0.000048	0.282346	7.6	−8.8	1.7	1,254
20.1	c	1,048	0.00138	0.05613	1.46707	0.00014	0.282443	0.000098	0.282416	10.6	−6.2	3.5	1,156
UNK.1	c[h]	1,050	0.00172	0.06145	1.46723	0.00018	0.281619	0.000081	0.281585	−18.8	−35.4	2.9	2,333
9.1	c	1,868	0.00120	0.03578	1.46714	0.00022	0.281282	0.000108	0.281240	−12.6	−47.2	3.8	2,763
R.2602.1 Joerg Peninsula													
1.1	r dark	237	0.00148	0.04878	1.46685	0.00032	0.282569	0.000046	0.282563	−2.2	−2.2	1.6	979
3.2	rim	237	0.00156	0.05285	1.46718	0.00053	0.282409	0.000043	0.282402	−7.9	−7.9	1.5	1,210
2.1	mixt	237	0.00241	0.10361	1.46708	0.00026	0.282410	0.000059	0.282399	−8.0	−8.0	2.1	1,237
8.1	oc bright	237	0.00287	0.08540	1.46715	0.00046	0.282440	0.000059	0.282427	−7.0	−7.0	2.1	1,209
Hf 8.1	r dark[g]	237	0.00289	0.11203	1.46722	0.00028	0.282433	0.000054	0.282421	−7.2	−7.2	1.9	1,219
8.1 rpt	r dark[g]	237	0.00224	0.07920	1.46712	0.00037	0.282453	0.000032	0.282443	−6.4	−6.4	1.1	1,170
9.1	oc bright	237	0.00120	0.04110	1.46719	0.00022	0.282560	0.000047	0.282555	−2.5	−2.5	1.7	985
11.1	oc bright	237	0.00150	0.04912	1.46721	0.00025	0.282619	0.000078	0.282612	−0.4	−0.4	2.8	909
13.2	r dark	237	0.00214	0.08812	1.46720	0.00028	0.282458	0.000031	0.282449	−6.2	−6.2	1.1	1,158
5.3	*r dark*	237	*0.00285*	*0.10507*	*1.46775*	*0.00048*	*0.282459*	*0.000076*	*0.282446*	*−6.3*	*−6.3*	*2.7*	*1,180*
4.1	oc bright	237	0.00227	0.09209	1.46725	0.00036	0.282446	0.000051	0.282435	−6.7	−6.7	1.8	1,181
13.1	c	497	0.00280	0.12063	1.46714	0.00031	0.282306	0.000068	0.282279	−6.5	−11.7	2.4	1,404
5.1	c	605	0.00189	0.07527	1.46709	0.00066	0.282319	0.000079	0.282297	−3.5	−11.1	2.8	1,351
3.1	c	1,037	0.00120	0.04734	1.46659	0.00079	0.282103	0.000102	0.282080	−1.6	−18.6	3.6	1,628
R.5257.1 Mount Eissenger													
hf gr 1	r[g]	228	0.00171	0.06271	1.46711	0.00021	0.282591	0.000046	0.282584	−1.6	−1.6	1.6	954
Hf gr2 r2	r[g]	228	0.00206	0.08518	1.46707	0.00027	0.282553	0.000048	0.282545	−3.0	−3.0	1.7	1,018
1.1	r	228	0.00212	0.07021	1.46704	0.00028	0.282743	0.000066	0.282734	3.7	3.7	2.3	744
11.1	r	228	0.00170	0.06719	1.46698	0.00028	0.282540	0.000058	0.282533	−3.5	−3.5	2.0	1,028
12.2	r	228	0.00233	0.06621	1.46741	0.00029	0.282653	0.000027	0.282643	0.5	0.5	1.0	880
13.2	r	228	0.00203	0.07242	1.46725	0.00028	0.282589	0.000027	0.282580	−1.8	−1.8	1.0	966
17.2	r	228	0.00171	0.08453	1.46699	0.00026	0.282558	0.000035	0.282551	−2.8	−2.8	1.2	1,001
20.1	r	228	0.00219	0.08073	1.46715	0.00026	0.282539	0.000056	0.282529	−3.6	−3.6	2.0	1,043
25.1	r	228	0.00199	0.07036	1.46711	0.00017	0.282633	0.000057	0.282625	−0.2	−0.2	2.0	901
25.1 rpt	r	228	0.00238	0.09814	1.46716	0.00020	0.282508	0.000041	0.282498	−4.7	−4.7	1.5	1,094
6.1	r	228	0.00259	0.10677	1.46739	0.00021	0.282655	0.000050	0.282644	0.5	0.5	1.8	883
14.1	r	228	0.00125	0.04791	1.46704	0.00031	0.282568	0.000063	0.282563	−2.4	−2.4	2.2	975
24.1	r	228	0.00379	0.12274	1.46730	0.00022	0.282521	0.000068	0.282505	−4.5	−4.5	2.4	1,118
hf gr 2	c[g]	422	0.00152	0.06869	1.46739	0.00026	0.282702	0.000040	0.282690	6.4	2.3	1.4	790
1.2	c	422	0.00170	0.08207	1.46745	0.00056	0.282836	0.000067	0.282823	11.1	7.0	2.4	601
12.1	c	422	0.00183	0.06848	1.46706	0.00026	0.282459	0.000085	0.282444	−2.3	−6.4	3.0	1,148
17.1	c	422	0.00246	0.10484	1.46729	0.00023	0.282481	0.000066	0.282461	−1.7	−5.7	2.3	1,136
18.1	c	422	0.00131	0.04482	1.46716	0.00026	0.282770	0.000096	0.282760	8.8	4.7	3.4	690
19.1	c	422	0.00176	0.07403	1.46719	0.00026	0.282648	0.000073	0.282634	4.4	0.4	2.6	873
2.1	c	422	0.00133	0.05312	1.46701	0.00025	0.282754	0.000094	0.282744	8.3	4.2	3.3	712
6.2	c	422	0.00154	0.06010	1.46734	0.00028	0.282580	0.000050	0.282568	2.1	−2.0	1.8	966
8.1	c	422	0.00144	0.06127	1.46698	0.00032	0.282680	0.000058	0.282669	5.6	1.5	2.0	821
5.1	c	1,043	0.00132	0.05336	1.46746	0.00036	0.282630	0.000054	0.282604	17.2	−0.2	1.9	890
R.4552.9 Mount Nordhill													
1.1	r	166	0.00092	0.02896	1.46710	0.00053	0.282441	0.000078	0.282439	−8.2	−8.2	2.8	1,144
Hf4	r	166	0.00074	0.02973	1.46719	0.00058	0.282455	0.000071	0.282453	−7.6	−7.6	2.5	1,120
Hf6.2	r	166	0.00136	0.06380	1.46729	0.00067	0.282361	0.000032	0.282357	−11.0	−11.0	1.1	1,271
Hf8.2	r	166	0.00146	0.04433	1.46761	0.00053	0.282440	0.000091	0.282435	−8.3	−8.3	3.2	1,164
Hf9.2	r	166	0.00080	0.03658	1.46735	0.00064	0.282478	0.000057	0.282475	−6.9	−6.9	2.0	1,090
Hf10.2	r	166	0.00060	0.02699	1.46728	0.00024	0.282507	0.000022	0.282505	−5.8	−5.8	0.8	1,044
4.1	*c*	*173*	*0.00092*	*0.03621*	*1.46734*	*0.00030*	*0.282716*	*0.000091*	*0.282713*	*1.7*	*1.6*	*3.2*	*759*

Table 2 (Contd.)

spot[a]	Analysis[b]	Age[c]	$^{176}Lu/^{177}Hf$	$^{176}Yb/^{177}Hf$	$^{178}Hf/^{177}Hf$	$\pm 2\sigma$	$^{176}Hf/^{177}Hf_m$	$\pm$ 2σ	$^{176}Hf/^{177}Hf_I$[d]	$EHf_{(t)}$[e]	$eHf_{(mig)}$[e]	$\pm 2\sigma$[e]	t_{DM} (Ma)[f]
27.1	c	182	0.00037	0.01259	1.46720	0.00058	0.282516	0.000102	0.282515	−4.9	−5.4	3.6	1,024
11.1	c	184	0.00107	0.04564	1.46732	0.00022	0.282602	0.000051	0.282599	−2.1	−2.5	1.8	922
7.1	*c*	*186*	*0.00030*	*0.01278*	*1.46692*	*0.00038*	*0.282471*	*0.000082*	*0.282470*	*−6.6*	*−7.1*	*2.9*	*1,086*
21.1	c	188	0.00041	0.01548	1.46710	0.00029	0.282518	0.000080	0.282517	−4.9	−5.4	2.8	1,023
8.1	*c*	*190*	*0.00026*	*0.01384*	*1.46703*	*0.00047*	*0.282370*	*0.000077*	*0.282369*	*−10.1*	*−10.6*	*2.7*	*1,223*
31.1	c	270	0.00059	0.02466	1.46720	0.00029	0.282372	0.000072	0.282369	−8.3	−10.6	2.5	1,231
6.1	c	329	0.00045	0.01943	1.46699	0.00032	0.282478	0.000060	0.282475	−3.3	−6.8	2.1	1,080
5.1	*c*	*389*	*0.00118*	*0.05383*	*1.46722*	*0.00027*	*0.282312*	*0.000052*	*0.282303*	*−8.0*	*−12.8*	*1.8*	*1,335*
28.1	c	830	0.00111	0.04261	1.46695	0.00018	0.282243	0.000057	0.282226	−1.0	−15.2	2.0	1,429
R.4293.1 Welch Mountains													
37.1	c	491	0.00024	0.01150	1.46724	0.00044	0.282623	0.000061	0.282621	5.5	−1.7	2.2	874
27.2	c	535	0.00104	0.04086	1.46706	0.00030	0.282421	0.000045	0.282411	−1.0	−8.9	1.6	1,177
11.1	c	551	0.00139	0.03866	1.46708	0.00031	0.282358	0.000061	0.282343	−3.1	−11.2	2.1	1,278
47.1	c	561	0.00024	0.01034	1.46698	0.00024	0.282372	0.000057	0.282369	−1.9	−10.5	2.0	1,220
34.1	c	578	0.00005	0.00246	1.46730	0.00027	0.282436	0.000055	0.282436	0.8	−8.2	1.9	1,126
18.1	c	595	0.00007	0.00451	1.46719	0.00027	0.282345	0.000056	0.282344	−2.0	−11.5	2.0	1,252
39.1	*c*	*599*	*0.00027*	*0.01100*	*1.46735*	*0.00023*	*0.282354*	*0.000043*	*0.282351*	*−1.7*	*−11.2*	*1.5*	*1,245*
43.1	c	624	0.00021	0.00916	1.46727	0.00025	0.282543	0.000069	0.282540	5.6	−4.5	2.5	984
46.1	*c*	*656*	*0.00076*	*0.03150*	*1.46718*	*0.00032*	*0.282453*	*0.000076*	*0.282443*	*2.8*	*−7.7*	*2.7*	*1,124*
42.1	c	657	0.00145	0.05586	1.46675	0.00031	0.282076	0.000043	0.282058	−10.8	−21.1	1.5	1,677
42.1 rpt	c	657	0.00148	0.06081	1.46713	0.00035	0.282307	0.000064	0.282289	−2.6	−13.0	2.3	1,352
32.1	c	663	0.00131	0.05430	1.46698	0.00029	0.282276	0.000064	0.282259	−3.5	−14.1	2.3	1,391
12.1	c	664	0.00073	0.02986	1.46714	0.00026	0.282388	0.000044	0.282379	0.7	−10.0	1.6	1,213
5.1	*c*	*678*	*0.00014*	*0.00749*	*1.46716*	*0.00042*	*0.282622*	*0.000054*	*0.282620*	*9.6*	*−1.7*	*1.9*	*873*
29.1	c	685	0.00084	0.03219	1.46715	0.00033	0.282463	0.000048	0.282452	3.8	−7.4	1.7	1,112
49.1	c	698	0.00123	0.05513	1.46696	0.00022	0.282301	0.000050	0.282285	−1.9	−13.2	1.8	1,352
15.1	*c*	*755*	*0.00092*	*0.03235*	*1.46718*	*0.00025*	*0.282316*	*0.000073*	*0.282303*	*0.1*	*−12.6*	*2.6*	*1,320*
26.1	c	787	0.00098	0.04165	1.46735	0.00028	0.282313	0.000059	0.282299	0.6	−12.7	2.1	1,326
9.1	c	930	0.00120	0.04456	1.46719	0.00028	0.282139	0.000058	0.282118	−2.6	−18.9	2.0	1,577
6.1	c	1,006	0.00260	0.09445	1.46707	0.00037	0.282271	0.000046	0.282222	2.8	−14.4	1.6	1,447
6.1 rpt	c	1,006	0.00224	0.09341	1.46703	0.00028	0.282275	0.000055	0.282233	3.2	−14.2	1.9	1,427
40.1	c	1,045	0.00077	0.03248	1.46677	0.00022	0.282258	0.000048	0.282243	4.4	−14.6	1.7	1,395
3.1	c	1,066	0.00129	0.05157	1.46729	0.00036	0.282370	0.000058	0.282344	8.5	−10.7	2.1	1,257
14.1	c	1,080	0.00058	0.02196	1.46746	0.00031	0.282257	0.000057	0.282245	5.3	−14.6	2.0	1,390
33.1	*c*	*1,087*	*0.00054*	*0.02271*	*1.46678*	*0.00028*	*0.282261*	*0.000062*	*0.282250*	*5.6*	*−14.5*	*2.2*	*1,383*
7.1	c	1,597	0.00164	0.06951	1.46727	0.00071	0.282054	0.000050	0.282004	8.4	−21.9	1.8	1,717
8.1	c	1,598	0.00268	0.09621	1.46696	0.00030	0.281918	0.000025	0.281837	2.4	−26.9	0.9	1,963
7.2	c	1,651	0.00290	0.12627	1.46670	0.00045	0.282050	0.000040	0.281959	8.0	−22.2	1.4	1,783
25.2	c	1,835	0.00078	0.03212	1.46709	0.00026	0.281689	0.000061	0.281661	1.6	−34.8	2.2	2,181

All uncertainties are given at the 2σ level. External precision based the reproducibility of the 91500 zircon standard from several analytical sessions, is approximately 2.3 epsilon units. Analyses in italics correspond to grains where the U–Pb age is poorly constrained, either by discordancy or large uncertainty

[a]Spot Identification number. rpt indicates replicate analysis on the same growth phase of the same zircon grain

[b]Portion of zircon analyzed where r = rim and c = core, r dark = dark outer rim, oc bright = CL-bright outer core

[c]Preferred U–Pb age from Table 1 or Millar et al. (2002)

[d]$^{176}Hf/^{177}Hf_{(i)}$ calculated using a Lu decay constant of 1.865×10^{-11} (Scherer et al. 2001)

[e]εHf values were calculated with $^{176}Hf/^{177}Hf$ and $^{176}Lu/^{177}Hf$ (CHUR) values of 0.282772 and 0.0332, respectively (Blichert-Toft and Albarède 1997). Measured 2σ errors average that indicated by the external reproducibility of the 91500 zircon standard

[f]Depleted mantle model ages were calculated using the measured $^{176}Lu/^{177}Hf$ of the zircon and present day $^{176}Hf/^{177}Hf$ and $^{176}Lu/^{177}Hf$ values of 0.28325 and 0.0384, respectively (Griffin et al. 2004)

[g]Indicates assumed age based on CL-patterns from other grains

[h]Age unknown

average value of 0.282447 ± 98 (2 SD, n = 6). Overall, the $^{176}Hf/^{177}Hf$ values for the cores are more variable than those of rims but on average, regardless of age, they are indistinguishable from those of the ca. 166 Ma rims (Fig. 6d), yielding values of 0.282460 ± 281 (2 SD, n = 10). Grains from the Welch Mountains sample yielded $^{176}Hf/^{177}Hf$ values that are generally lower than those of the Mount Nordhill rims (Fig. 6d).

Hf isotopes, anatexis and the source of crustal melts

At the site of crustal melting, hafnium within the melt is either derived from (a) dissolved zircon or, (b) the breakdown of less hafnium-rich minerals such as titanite, amphibole, pyroxene and other accessory minerals. This second source of hafnium is particularly important

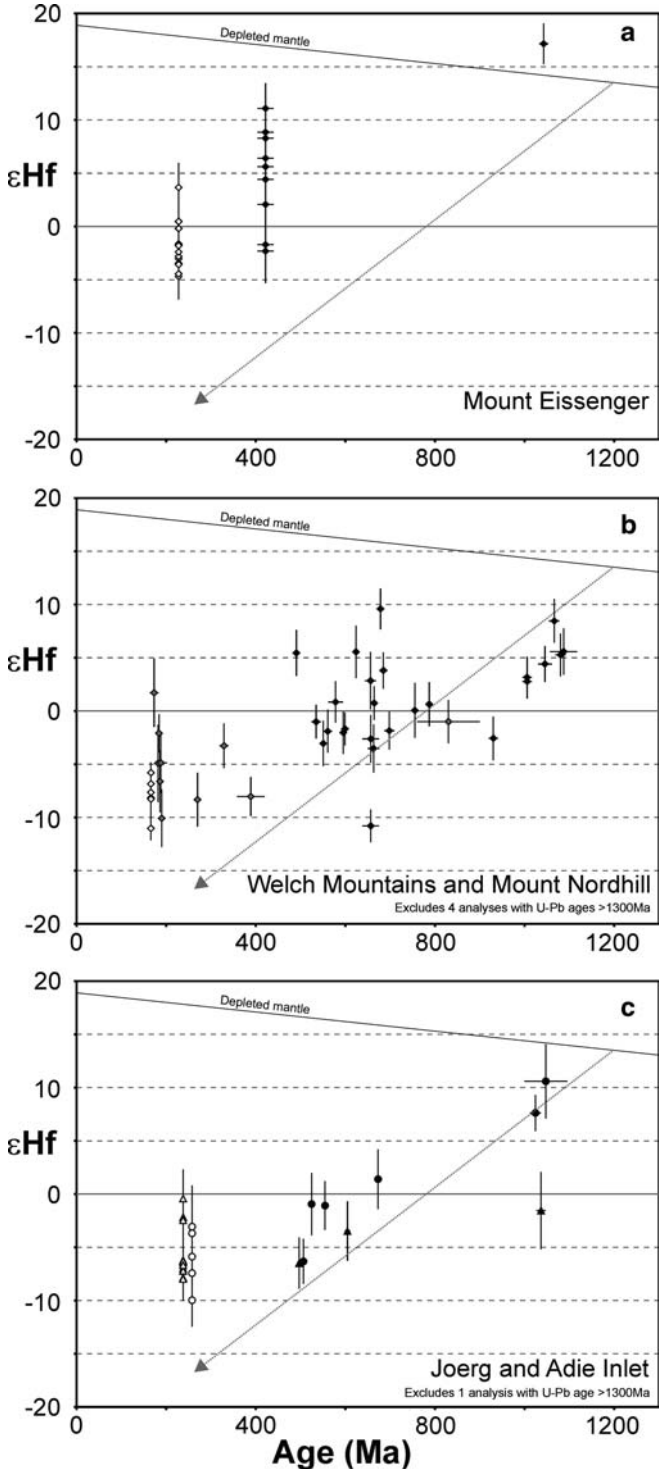

Fig. 7 εHf versus $^{206}Pb/^{238}U$ age plots of zircons from the studied granites and migmatites. **a** *Solid diamonds*: Mount Eissenger inherited. *Open diamond*: Mount Eissenger rims. **b** *Solid diamonds*: Welch Mountains detrital. *Grey diamonds*: Mount Nordhill inherited. *Open diamonds*: Mount Nordhill rims. **c** *Solid triangles*: Joerg inherited. *Open triangles*: Joerg rims. *Solid circles*: Adie Inlet inherited. *Open circles* Adie Inlet rims. The *arrow* indicates evolution of a zircon with a $^{176}Lu/^{177}Hf$ of 0.0015, a typical values for the grains analyzed in this study. *Error bars* are given at the 2σ level

where the source rock is zircon poor. A significant factor that needs to be considered for non-zircon sources of hafnium is that they also contain higher concentrations of lutetium and so may have significantly higher $^{176}Hf/^{177}Hf$ than that derived from zircon in the same rock.

The range of hafnium values obtained from zircon that grew from a melt determine how isotopically homogenous it was. When these values are compared with those from the inherited component together with an assessment of zircon texture, an analysis of the anatectic processes at work can be made. For instance, if every zircon that grew from a particular melt had an identical Hf-isotope signature one could assume that the melt was isotopically homogenous. If this Hf-isotope signature is indistinguishable from the inherited component and there is abundant textural evidence for zircon dissolution, in situ melting and a closed system is indicated. Isotopic heterogeneity of zircons that grew from a particular melt would be indicated by significant variation in their Hf-isotope composition. In such instances, mixing from isotopically different sources and that each zircon is sampling small melt volumes could be implied.

Examining the textures and the range of $^{176}Hf/^{177}Hf$ in the zircons and any inherited component can therefore determine the degrees of melt homogeneity and the degree of mixing from isotopically different sources. In the sections below an attempt is made to assess the most likely sources and processes in operation during the generation of crustal melts in the Antarctic Peninsula.

Hf isotopes from samples with abundant inherited zircon and dissolution textures

Based on the study of Williams (2001), the zircon core–rim textures from both the Mount Eissenger leucosome and Mount Nordhill leucocratic gneiss samples demonstrate that the cores were partially dissolved in a melt before the growth of the rims. Without doubt, this texture indicates that Hf must have been liberated into the melt by zircon dissolution during migmatization. For these two samples, irrespective of age, the core and rim εHf and $^{176}Hf/^{177}Hf$ are, on average, indistinguishable. This observation is consistent with the Hf budget of the melt being controlled by zircon dissolution and that the proportion of Hf released from the zircon was large enough to swamp that derived from other sources.

Although the averages are identical, there is significant scatter in core and rim values suggesting relict isotopic heterogeneity is preserved from the inherited source(s) and in the melt. Generally, the spread in $^{176}Hf/^{177}Hf$ is less for the rims than the cores (Fig. 7a, b) but the rims exhibit a larger range of $^{176}Hf/^{177}Hf$ than one might expect from closed system melting and homogenization. However, excluding single outlying

results from both the Mount Eissenger leucosome and Mount Nordhill leucocratic gneiss samples, the rims have $^{176}Hf/^{177}Hf$ compositions that are, within a range of 5 epsilon units, consistent from grain to grain (Fig. 7a, b). This suggests some isotopic homogenization occurred within the melt. For example, consider individual zircon grains from the Mount Eissenger leucosome sample that yield core and the rim analyses which differ by more than analytical uncertainty. Core analyses that yield extreme εHf values, at either end of the range measured for all the inherited grains, have corresponding rim analyses that sit within the main cluster of analyses (grains 12 and Hf grain 2; Table 2). Assuming the Hf budget is largely controlled by the dissolved zircon, had mixing and homogenization not occurred, then the rim analyses should also have yielded extreme εHf values, at either end of the range. Therefore a degree of Hf isotope homogenization was achieved in the melt.

The following hypothesis is proposed for the Mount Eissenger and Mount Nordhill samples: zircons that crystallized from the melt scavenged their elemental Hf and Hf isotope signatures primarily from zircon dissolved during anatexis. Some of this zircon survived as a partially dissolved inherited component in the melt. The rims are likely to record the $^{176}Hf/^{177}Hf$ of the melt; if Hf-rich minerals other than zircon contributed to the Hf budget of the melt, they had $^{176}Hf/^{177}Hf$ indistinguishable from the range of $^{176}Hf/^{177}Hf$ values measured in the inherited zircon, and thus the two possible sources cannot be distinguished. During anatexis, some degree of Hf isotope homogeneity was most likely achieved through small-scale melt migration. Complete Hf isotope homogeneity was not achieved and some zircon possibly grew from small melt volumes that either preserved isotope heterogeneity from a single protolith or, more likely, melt sourced from different protoliths each with a different isotope character.

More specifically, the Mount Eissenger leucosome has a simple zircon inheritance, either from a single ca. 422 Ma protolith with a large Hf-isotope variation, or several ca. 422 Ma protoliths with different Hf isotope compositions. Magmatic zircons that crystallized in the leucosome have, on average, $\varepsilon Hf_{(227)}$ of −1.8, corresponding to a t_{DM} model age of 970 Ma, which is indistinguishable from the average t_{DM} Hf model age of the inherited zircon component and broadly equates to the t_{DM} Nd model age of ∼ 1,030 Ma. Therefore Hf isotopes of the inherited and magmatic zircon components indicate in situ melting.

The ages and age distribution patterns of the inherited zircon from the Welch Mountains paragneiss are not consistent with it being a source for the Mount Nordhill gneissic leucocratic sheet (Wever et al. 1994; Fig. 4); inherited zircon in the Mount Nordhill gneissic leucogranite is dominated by ca. 180 Ma zircons, whereas the Welch Mountains paragneiss is dominated by 500–600 Ma and older zircons. Although less conclusive than the U–Pb data, the small difference in the t_{DM} Nd model ages for the Welch Mountains paragneiss and the Mount Nordhill Leucocratic gneiss is consistent with this interpretation. Like the Nd data, the Hf isotope composition of the Welch Mountains paragneiss detrital zircon grains are, on average, more evolved than both the inherited and magmatic zircon from the leucocratic sheet. However, the Hf isotope data do not rule-out the Welch Mountains paragneiss as a contributing source. For the Hf primarily derived from minerals other than zircon, evolution of the whole rock (an approximation of the Hf isotope composition from such minerals) prior to metamorphism could account for the resultant, more juvenile, Hf isotope composition of the zircon rims from the Mount Nordhill leucocratic gneiss. However, textural evidence, as argued above, suggests this was not the case and that the dissolved zircon controlled the Hf budget of the melt. Altogether, the geochronological and isotope data reveal that melting was of a sedimentary source(s) and that melt transport has emplaced the sheet into the Welch Mountains paragneiss. The source is either not exposed or has not been recognized.

Hf isotopes from samples with abundant inherited zircon but limited dissolution

On textural grounds, it is clear that the dissolution of inherited zircon during anatexis is less pronounced for the Adie Inlet gneiss sample. Commonly, new zircon overgrew rounded and elongate inherited grains and only rarely are there examples of irregular interfaces between core and rim that are indicative of zircon dissolution, suggesting that that rims may have overgrown originally detrital grains contained within the gneiss. Like the Mount Eissenger and Mount Nordhill samples, the rims have a degree of variation in their $^{176}Hf/^{177}Hf$ compositions from grain to grain. This variation is less than that recorded from the inherited component (Fig. 7c), indicating that the Hf isotopes within the melt were also partially homogenized.

Inspection of the average $^{176}Hf/^{177}Hf$ values of the cores and rims, suggest that the zircon rims require a less-evolved component than can be obtained from the inherited cores (Fig. 6a). This could suggest an open system and mixing of melt derived from the isotopically distinct domains within the Adie Inlet gneisses, as indicated by Sr and Nd whole rock geochemistry, with that derived from the inherited zircon component. Given that less zircon dissolution occurred during anatexis, derivation of some Hf from minerals other than zircon would be more likely to influence the Hf budget of the melt and may also account for the apparently more juvenile rims. We suspect that the Adie Inlet gneiss formed at least in part by in situ melting of its protolith(s), and that the inherited zircons contributed some of the Hf to the melt, as is indicated from rare dissolution textures seen in the CL images, but until further work is carried out, the evolution of the Adie Inlet gneiss remains unclear.

Hf isotopes from samples with rare inherited zircon

The low abundance of inherited zircon within the Joerg Peninsula gneiss sample suggests that it represents a discrete granitoid intrusion rather than the product of localized anatexis and migmatite formation. Intrusion was likely to be complex given the generation of distinct early luminescent inner and later non-luminescent rims. This zircon texture could indicate multiple phases of intrusion in the mid-Triassic, at 238 ± 5 Ma. The Hf isotope compositions for luminescent and non-luminescent Triassic growth phases are, on average, indistinguishable, suggesting a common source. However, both types of zircon exhibit a range of $^{176}Hf/^{177}Hf$ that equates to 8 epsilon units (Fig. 7c). Such variation supports the possibility of partially mixing of magma batches, each with a distinct Hf isotope composition. The inherited zircons have much lower $^{176}Hf/^{177}Hf$ (Fig. 6b), and due to their low abundance, could have been picked up from wall rock during ascent and emplacement of the granite magma. Like the Adie inlet sample, a contribution from minerals other than zircon could account for the juvenile character of the Triassic zircon. However, the lack of zircon inheritance does not permit further exploration.

New U–Pb zircon geochronology and Hf isotopes analyses of zircon in the context of the evolution of the Antarctic Peninsula

The detrital zircon age patterns and Hf isotope signatures from the Welch Mountains paragneiss shows that the detrital zircons with an age of ca. 1,200 Ma and younger were originally formed from material with an average mantle separation age of approximately 1,300 Ma (Fig. 7a). Crust of this age, with εHf of ca. +10 at 1,200 Ma (BAS unpublished data), is exposed at Haag Nunataks, situated approximately 750 km southwest from the Welch Mountains in Eastern Ellsworth Land. Based on Nd and Sr isotope ratios it has long been proposed that crust with a similar isotope signature was involved in the petrogenesis of Antarctic Peninsula granitoids (e.g., Millar et al. 2001). Should these zircons be derived from basement to the Antarctic Peninsula, then our Hf isotope data support the conclusions reached from the Nd and Sr data. Importantly, some of the zircon populations can be further subdivided based on their Hf isotope signature. For instance, the ca. 662 Ma population (zircons with $^{206}Pb/^{238}U$ ages within error of 662 Ma) has zircons with εHf values of approximately 2.5 and could have formed by the reworking crust like that at Haag Nunataks. The population also contains several zircon grains that are less-evolved and require a source that is either a mixture of that derived from crust like that at Haag Nunataks and a less-evolved, possibly mantle-derived source, or a different, more juvenile source than that at Haag Nunataks. One zircon grain yields a much more negative εHf value of −10.8 (Fig. 7b). Although this zircon crystallized at ca. 662 Ma, the negative εHf value suggests that the melt was predominantly sourced from Palaeoproterozoic material and therefore probably originated from crust outside of the Antarctic Peninsula. As a note of caution, the other detrital grains could also be recycled in the sedimentary system and have also originated from outside of the Antarctic Peninsula.

For the Adie Inlet gneiss, one 1,868 Ma grain with εHf of −11 requires an Archaean crustal source (Table 2). In a reconstruction of Gondwana, the closest potential source for zircons of this age would be in the Kaapvaal craton in Southern Africa (Poujol et al. 2003). Whether the zircons were recycled several times before being entrained in the Adie Inlet gneiss or originate from first cycle sedimentation cannot be resolved.

Although the cores of Mount Eissenger zircons are similar in age, they display a wide variation in εHf ratio (Fig. 7b). Such variation is statistically significant. An alternative to the possibility that the inherited grains represent zircon grains derived from different sources with distinct Hf isotope compositions, is that the variation represents temporal changes in $^{176}Hf/^{177}Hf$ in the magma chamber of the original igneous protolith during zircon crystallization. Such isotope variation probably reflects entrainment of different batches of magma with differing sources and Hf isotope ratios into the chamber. A similar variation in $^{176}Hf/^{177}Hf$ for zircon described by Griffin et al. (2002) is also attributed to magma mixing.

The new U–Pb age of 238 ± 5 Ma for the Joerg Peninsula orthogneiss is in agreement with the previously determined whole rock Rb–Sr isochron of 236 ± 7 Ma (Hole et al. 1991). The 166 ± 3 Ma for the age of the Mount Nordhill leucocratic dyke is unexpected, as the age of migmatization was expected to be comparable to the Triassic ca. 230 Ma or earliest Jurassic ca. 205 Ma events that are recorded in northeast Palmer Land (Millar et al. 2002). How widespread the *c.* 166 Ma metamorphism is, is at present, unclear. However, given the large quantity of ca. 180 Ma inherited zircon, the event post-dated initial magmatism related to the breakup of Gondwana, although overlapped with later silicic volcanism associated with the breakup (Silicic phase V2 of Pankhurst et al. 2000). Therefore, this event may represent decompression melting during uplift, facilitated by crustal extension and high heat flow that followed separation of the eastern Antarctic Peninsula from Gondwana.

Conclusions

We have measured the Hf isotope ratios of zircon by LA–MC–ICP–MS from four different samples of migmatite and granite gneiss and one possible migmatite-source rock from the Antarctic Peninsula. We have

also presented SHRIMP U–Pb zircon geochronology for the samples where age information for the analyzed rocks is not already available. Our results show that Hf isotope studies offer potential for future investigation into the sources of crustal melts. For these samples studied from the Antarctic Peninsula:

1. Zircon from migmatite and granite gneiss samples are complex and display core and rim structures under CL. The cores are older inherited zircon components that have suffered variable amounts of dissolution during anatexis. The rims are the same age and are interpreted to have grown from the melt generated during metamorphism.
2. Zircon rims have $^{176}Hf/^{177}Hf$ that are similar from grain to grain in each sample. Significant isotopic variation is present but variation is less pronounced in the newly grown zircon than the inherited zircon and suggests Hf-isotope homogenization, possibly caused by melt migration. The variation preserved in the zircon rims may represent partial mixing of Hf derived from separate, isotopically distinct sources, or preserve original source heterogeneity.
3. Where textural evidence suggests large degrees of dissolution of the inherited zircon component (Mount Eissenger leucosome and Mount Nordhill leucocratic gneiss samples), the $^{176}Hf/^{177}Hf$ of the inherited and newly grown zircon from the melt are, on average, indistinguishable. We suggest that the Hf budget was controlled by the dissolved zircon component and similar zircon at the source, and that the system was largely closed. The Mount Eissenger sample therefore probably records in situ migmatization at ca. 227 Ma of a ca. 422 Ma protolith. The Mount Nordhill sample does not have a Welch Mountains paragneiss source, as the paragneiss does not contain zircon signatures compatible with the inherited zircon age pattern. Melt migration allowed intrusion into the Welch Mountains paragneiss at 166 ± 3 Ma. Metamorphism and melt generation at ca. 166 Ma might reflect either high heat flow related to the generation of large volumes of plume-related silicic volcanism at this time or decompression melting following the break away of the eastern Antarctic Peninsula from Gondwana.
4. Where textural evidence suggests that the inherited zircon has undergone smaller degrees of dissolution during anatexis (Adie Inlet gneiss and Joerg Peninsula gneiss samples), the $^{176}Hf/^{177}Hf$ values of the inherited and newly grown zircon are different. In both cases the melt apparently requires an additional, less evolved, source but can also be accounted for by Hf derived from minerals other than zircon, which because of their lutetium content may have evolved a higher $^{176}Hf/^{177}Hf$ than that of the average inherited zircon component. The evolution of these samples remains uncertain but the Adie Inlet gneiss may represent invasion of a melt derived from adjacent protoliths that are less evolved than the gneiss itself. The Joerg Peninsula gneiss probably reflects multiple intrusions of melt from a source with a somewhat variable Hf isotope composition, at 238 ± 5 Ma. Inherited zircon within the Joerg Peninsula gneiss may have resulted from wall-rock contamination during ascent and emplacement of the magma.
5. Hf isotopes of inherited zircons from all rocks, irrespective of age, were predominantly formed from melt derived from sources with late Mesoproterozoic mantle extraction ages.

Acknowledgements MJF acknowledges support from the Antarctic Funding Initiative (grant AFI 3/13 awarded to ILM and APMV) and skilled laboratory assistance by Vanessa Pashley at NIGL. ILM and APMV are indebted to the tireless assistance of the BAS operations group and field assistants that make fieldwork and sample collection in Antarctica possible. This work is a contribution to the BAS core programme Antarctica in the Dynamic Global Plate System, in particular the project Superterranes in the Pacific-margin arc (SPARC). Thorough and instructive reviews by Nigel Kelly and Tony Kemp and patient editing by Ian Parsons are greatly appreciated and have improved an earlier version of this manuscript.

References

Andersen T, Griffin WL (2004) Lu–Hf and U–Pb isotope systematics of zircons from the Storgangen intrusion, Rogaland Intrusive Complex, SW Norway: implications for the composition and evolution of Precambrian lower crust in the Baltic Shield. Lithos 73:271–288

Andersen T, Griffin WL, Pearson NJ (2002) Crustal evolution in SW part of the Baltic Shield; the Hf isotope evidence. J Petrol 43:1725–1747

Blichert-Toft J, Albarède F (1997) The Lu–Hf isotope geochemistry of chrondrites and the evolution of the mantle-crust system. Earth Planet Sci Lett 148:243–258

Chu NC, Taylor RN, Chavagnac V, Nesbitt RW, Boella RM, Milton JA, German CR, Bayon G, Burton K (2002) Hf isotope ratio analysis using multi-collector inductively coupled plasma mass spectrometry: an evaluation of isobaric interference corrections. J Anal At Spectrom 17:1567–1574

Clemens JD (2003) S-type granitic magmas—petrogenetic issues, models and evidence. Earth Sci Rev 61:1–18

Corfu F, Noble SR (1992) Genesis of the southern Abitibi greenstone belt, Superior Province, Canada: evidence from zircon Hf isotope analysis using a single filament technique. Geochim Cosmochim Acta 56:2081–2097

Griffin WL, Pearson NJ, Belousova E, Jackson SE, van Achterbergh E, O'Reilly SY, Shee SR (2000) The Hf isotope composition of cratonic mantle; LAM-MC-ICPMS analysis of zircon megacrysts in kimberlites. Geochim Cosmochim Acta 64:133–147

Griffin WL, Wang X, Jackson SE, Pearson NJ, O'Reilly SY, Xu X, Zhou X (2002) Zircon chemistry and magma mixing, SE China: in situ analysis of Hf isotopes, Tonglu and Pingtan igneous complexes. Lithos 61:237–269

Griffin WL, Belousova EA, Shee SR, Pearson NJ, O'Reilly SY (2004) Archean crustal evolution in the northern Yilgarn Craton: U–Pb and H-isotope evidence from detrital zircons. Precambrian Res 131:231–282

Halpin JA, Gerakiteys CL, Clarke GL, Belousova EA, Griffin WL (2005) In situ U–Pb geochronology and Hf isotope analyses of the Rayner Complex, east Antarctica. Contrib Mineral Petrol 148:689–706

Hole MJ (1986) Time controlled geochemistry of igneous rocks of the Antarctic Peninsula. Unpublished Ph.D. thesis, University of London

Hole MJ, Pankhurst RJ, Saunders AD (1991) Geochemical evolution of the Antarctic Peninsula magmatic arc: the importance of mantle-crust interactions during granitoid genesis. In: Thomson MRA, Crame JA, Thomson JW (eds) Geological evolution of Antarctica. Cambridge University Press, London, pp 369–374

Horstwood MSA, Foster GL, Parrish RR, Noble SR, Nowell GM (2003) Common-Pb corrected in situ U–Pb accessory mineral geochronology by LA–MC–ICP–MS. J Anal At Spectrom 18:837–846

Hoskin PWO, Schaltegger U (2003) The composition of zircon and igneous and metamorphic petrogenesis. In: Hanchar JM, Hoskin PWO (eds) Zircon. Reviews in mineralogy and geochemistry vol 53. Mineralogical society of America, Geochemical Society, pp 27–62

Kinny PD, Compston W, Williams IS (1991) A reconnaissance ion-probe study of hafnium isotopes in zircons. Geochim Cosmochim Acta 55:849–859

Knudsen TL, Griffin WL, Hartz EH, Andersen A, Jackson SE (2001) In situ hafnium and Pb isotope analyses of detrital zircons from the Devonian sedimentary basin from NE Greenland: a record of repeated crustal reworking. Contrib Mineral Petrol 141:83–94

Leat PT, Scarrow JH, Millar IL (1995) On the Antarctic Peninsula batholith. Geol Mag 132:399–412

Ludwig K (1999) Isoplot/Ex, a geochronological toolkit for Microsoft Excel, version 2.31. Berkeley Geochronological Centre Special Publications, 1, Berkeley Geochronological Centre, 2455 Ridge Road, Berkeley, California 94709

Maas R, Nicholls IA, Greig A, Nemchin A (2001) U–Pb zircon studies of mid-crustal metasedimentary enclaves from the S-Type Deddick Granodiorite, Lachlan Fold Belt, SE Australia. J Petrol 42:1429–1448

Millar IL, Willan RCR, Wareham CD, Boyce AJ (2001) The role of crustal and mantle sources in the genesis of granitoids of the Antarctic Peninsula and adjacent crustal blocks. J Geol Soc London 158:855–868

Millar IL, Pankhurst RJ, Fanning CM (2002) Basement chronology and the Antarctic Peninsula: recurrent magmatism and anatexis in the Palaeozoic Gondwana Margin. J Geol Soc London 159:145–158

Nowell G, Parrish RR (2001) Simultaneous acquisition of isotope compositions and parent/daughter ratios by non-isotope dilution solution-mode plasma ionisation multi-collector mass spectrometry (PIMMS). In: Holland JG, Tanner SD (eds) Plasma source spectrometry: the new Millennium Special Volume, Royal Society of Chemi1stry, London, pp 267

Nowell GM, Kempton PD, Noble SR, Fitton JG, Saunders AD, Mahoney JJ, Taylor RN (1998) High precision Hf isotope measurements of MORB and OIB by thermal ionisation mass spectrometry: insights into the depleted mantle. Chem Geol 149:211–233

Pankhurst RJ (1983) Rb–Sr constraints on the ages of basement rocks of the Antarctic Peninsula. In: Oliver RL, James PR, Jago JB (eds) Antarctic earth sciences. Cambridge University Press, London, pp 367–371

Pankhurst RJ, Riley TR, Fanning CM, Kelley SP (2000) Episodic silicic volcanism in Patagonia and the Antarctic Peninsula: chronology of magmatism associated with the break-up of Gondwana. J Petrol 41:605–625

Paterson BA, Stephens WE, Rogers G, Williams IS, Hinton RW, Herd DA (1992) The nature of zircon inheritance in two granite plutons. Trans R Soc Edinb Earth Sci 83:459–471

Pidgeon RT, Compston W (1992) A SHRIMP ion microprobe study of inherited and magmatic zircons from four Scottish Caledonian granites. Trans R Soc Edinb Earth Sci 83:473–483

Piercy BA, Harrison SM (1991) Mesozoic metamorphism, deformation and plutonism in the southern Antarctic Peninsula: evidence from north-western Palmer Land. In: Thomson MRA, Crame JA, Thomson JW (eds) Geological evolution of Antarctica. Cambridge University Press, London, pp 381–385

Poujol M, Robb LJ, Anhaeusser CR, Gericke B (2003) A review of the geochronological constraints on the evolution of the Kaapvaal Craton, South Africa. Precambrian Res 127:181–213

Rex D (1976) Geochronology in relation to stratigraphy of the Antarctic Peninsula. Br Antarct Surv Bull 43:49–58

Scherer E, Münker C, Mezger K (2001) Calibration of the lutetium hafnium clock. Science 293:683–687

Scherstén A, Larson SÅ, Cornell DH, Stigh J (2004) Ion probe dating of a migmatite in SW Sweden: the fate of zircon in crustal processes. Precambrian Res 130:251–266

Schmitz MD, Bowring SA, Ireland TR (2003) Evaluation of Duluth Complex anorthositic series (AS3) zircon as a U–Pb geochronological standard: new high-precision isotope dilution mass spectrometry results. Geochim Cosmochim Acta 67:3665–3672

Singleton DG (1980) The geology of the central Black Coast, Palmer Land. Br Antarct Surv Sci Rep 102:54

Smith PE, Tatsumoto M, Farquhar RM (1987) Zircon Lu–Hf systematics and the evolution of the Archean crust in the Superior Province, Canada. Contrib Mineral Petrol 97:93–104

Steiger RH, Jäger E (1977) Subcommission on geochronology; convention on the use of decay constants in geo- and cosmochronology. Earth Planet Sci Lett 36:359–362

Storey BC (1991) The crustal blocks of West Antarctica within Gondwana: reconstruction and break-up model. In: Thomson MRA, Crame JA, Thomson JW (eds) Geological evolution of Antarctica. Cambridge University Press, London, pp 587–592

Storey BC, Dalziel IWD, Garrett SW, Grunow AM, Pankhurst RJ, Vennum WR (1988) West Antarctica in Gondwanaland: crustal blocks, reconstruction and breakup processes. Tectonophysics 155:381–390

Suárez M (1976) Plate tectonic model for southern Antarctic Peninsula and its relation to southern Andes. Geology 4:211–214

Thirlwall MF, Walder AJ (1995) In situ hafnium isotope ratio analysis of zircon by inductively coupled plasma multiple collector mass spectrometry. Chem Geol 122:241–247

Thompson MRA, Pankhurst RJ (1983) Age of post-Gondwanan calc-alkaline volcanism in the Antarctic Peninsula region. In: Oliver RL, James PR, Jago JB (eds) Antarctic Earth Sciences. Cambridge University Press, London, pp 328–333

Tikhomirova M (2002) Zircon inheritance in diatexite granodiorites and its consequence on geochronology—a case study in Lusatia and the Erzgebirge (Saxo-Thuringia, eastern Germany). Chem Geol 191:209–224

Vaughan APM, Millar IL (1996) Early cretaceous magmatism during extensional deformation within the Antarctic Peninsula Magmatic Arc. J South Am Earth Sci 9:121–130

Vaughan APM, Storey BC (2000) The eastern Palmer Land shear zone: a new terrane accretion model for the Mesozoic development of the Antarctic Peninsula. J Geol Soc London 157:1243–1256

Vaughan APM, Wareham CD, Millar IL (1997) Granitoid pluton formation by spreading of continental crust: the Wiley Glacier complex, northwest Palmer Land, Antarctica. Tectonophysics 283:35–60

Vaughan APM, Pankhurst RJ, Fanning CM (2002) A mid-Cretaceous age for the Palmer Land event, Antarctic Peninsula: implications for terrane accretion timing and Gondwana palaeolatitudes. J Geol Soc London 159:113–116

Veevers JJ, Saeed A, Belousova EA, Griffin WL (2005) U–Pb ages and source composition by Hf-isotope and trace-element analysis of detrital zircons in Permian sandstone and modern sand from southwestern Australia and a review of the palaeogeographical and denudational history of the Yilgarn Craton. Earth Sci Rev 68:245–279

Watson EB, Harrison TM (1983) Zircon saturation revisited: temperature and composition effects in a variety of crustal magma types. Earth Planet Sci Lett 64:295–304

Wever HE, Millar IL, Pankhurst RJ (1994) Geochronology and radiogenic isotope geology of Mesozoic rocks from eastern Palmer Land, Antarctic Peninsula; crustal anatexis in arc-related granitoid genesis. J South Am Earth Sci 7:69–83

Wever HE, Storey BC, Leat PT (1995) Peraluminous granites in NE Palmer Land, Antarctic Peninsula; early Mesozoic crustal melting in a magmatic arc. J Geol Soc London 152:85–96

Whitehouse MJ, Kamber BS (2003) A rare earth element study of complex zircons from early Archaean Amitsoq gneisses, Godthabsfjord, south-west Greenland. Precambrian Res 126:363–377

Wiedenbeck M, Alle P, Corfu F, Griffin WL, Meirer M, Oberli F, Von Quadt A, Roddick JC, Spiegel W (1995) Three natural zircon standards for U–Th–Pb, Lu–Hf, trace element and REE analyses. Geostandard Newsl 19:1–23

Williams IS (1995) Zircon analysis by ion microprobe: the case of the eastern Australian granites. Leon T. Silver 70th birthday celebration, The California Institute of Technology, pp 27–31

Williams IS (1998) U–Th–Pb geochronology by ion microprobe. In: McKibben MA, Shanks WC, Ridley WI (eds) Applications of microanalytical techniques to understanding mineralizing processes. Reviews in Economic Geology, Society of Economic Geologists, Socorro, New Mexico, pp 1–35

Williams IS (2001) Response of detrital zircon and monazite, and their U–Pb isotopic systems, to regional metamorphism and host-rock partial melting, Cooma Complex, southeastern Australia. Aust J Earth Sci 48:557–580

Williams IS, Claesson S (1987) Isotopic evidence for the Precambrian provenance and Caledonian metamorphism of high grade paragneisses from the Seve Nappes, Scandinavian Caledonides. Contrib Mineral Petrol 97:205–217

Woodhead J, Hergt J, Shelley M, Eggins S, Kemp R (2004) Zircon Hf-isotope analysis with an excimer laser, depth profiling, ablation of complex geometries, and concomitant age estimation. Chem Geol 209:121–135

Zeck HP, Williams IS (2002) Inherited and magmatic zircon from Neogene Hoyazo cordierite dacite, SE Spain; anatectic source rock provenance and magmatic evolution. J Petrol 43:1089–1104

Zheng J, Griffin WL, O'Reilly SY, Lu F, Yu C, Zhang M, Li H (2004) U–Pb and Hf-isotope analysis of zircons in mafic xenoliths from Fuxian kimberlites: evolution of the lower crust beneath the north China craton. Contrib Mineral Petrol 148:79–103